



Published in final edited form as:

Phys Med Biol. 2015 July 21; 60(14): R239–R269. doi:10.1088/0031-9155/60/14/R239.

Quantitative *in vivo* cell-surface receptor imaging in oncology: kinetic modeling & paired-agent principles from nuclear medicine and optical imaging

Kenneth M. Tichauer¹, Yu Wang², Brian W. Pogue³, and Jonathan T. C. Liu²

¹Biomedical Engineering, Illinois Institute of Technology, Chicago IL 60616

²Mechanical Engineering, University of Washington, Seattle WA 98195

³Thayer School of Engineering, Dartmouth College, Hanover NH 03755

Abstract

The development of methods to accurately quantify cell-surface receptors in living tissues would have a seminal impact in oncology. For example, accurate measures of receptor density *in vivo* could enhance early detection or surgical resection of tumors via protein-based contrast, allowing removal of cancer with high phenotype specificity. Alternatively, accurate receptor expression estimation could be used as a biomarker to guide patient-specific clinical oncology targeting of the same molecular pathway. Unfortunately, conventional molecular contrast-based imaging approaches are not well adapted to accurately estimating the nanomolar-level cell-surface receptor concentrations in tumors, as most images are dominated by nonspecific sources of contrast such as high vascular permeability and lymphatic inhibition. This article reviews approaches for overcoming these limitations based upon tracer kinetic modeling and the use of emerging protocols to estimate binding potential and the related receptor concentration. Methods such as using single time point imaging or a reference-tissue approach tend to have low accuracy in tumors, whereas paired-agent methods or advanced kinetic analyses are more promising to eliminate the dominance of interstitial space in the signals. Nuclear medicine and optical molecular imaging are the primary modalities used, as they have the nanomolar level sensitivity needed to quantify cell-surface receptor concentrations present in tissue, although each likely has a different clinical niche.

1. Introduction

Cell-surface receptors that are specific to, or overexpressed by, cancer cells have been a critical target of interest in oncological research for decades (Gambhir, 2002; Weissleder, 2006). The overexpression, mutation, and selective expression of cell-surface receptors in cancer compared to healthy tissue were first observed through serological tests of cancer in the 1960s (Rettig and Old, 1989; van den Eynde and Scott, 1998). Since then, the identification of these receptors through medical imaging technologies (*i.e.* “molecular imaging”) has been proposed as a means of significantly improving many aspects of cancer management, including (1) enabling more sensitive and early detection of cancer at the molecular level (Massoud and Gambhir, 2003; Schottelius and Wester, 2009; Yang *et al.*, 2006), (2) improving the delineation of tumor from healthy tissue during cancer surgery (Liu

et al., 2014; Vahrmeijer *et al.*, 2013), and (3) revealing accessible molecular targets for cancer-specific pharmaceuticals (Brannon-Peppas and Blanchette, 2012; de Wiele *et al.*, 2008). The utility of molecular imaging with respect to cancer diagnosis and image-guided surgery (example 1 and 2 above) is obvious. In targeted-drug applications (example 3), biopsies are often obtained to analyze the molecular status of a patient's cancer in order to guide and personalize a therapeutic regimen (Baloch *et al.*, 2008; DeMarzo *et al.*, 2003; Rouzier *et al.*, 2005). However, recent studies have observed significant intra-tumor spatial heterogeneity in molecular biomarker expression, as well as variations in expression patterns over time, suggesting that a regional biopsy at a fixed time point may not be representative of the complete disease (van den Eynde and Scott, 1998; Fidler, 1978; Gerlinger *et al.*, 2012; Longo, 2012). In response, *in vivo* molecular imaging approaches have been proposed to comprehensively examine the molecular profile of entire tumors (including satellite sites), potentially over time, to better guide personalized treatments (Weissleder and Pittet, 2008).

Significant advances have been achieved over the years with respect to imaging and identifying receptors in tissues, with the vast majority of these studies being carried out using nuclear medicine or optical imaging modalities since conventional magnetic resonance imaging and x-ray computed tomography are typically unable to offer the level of molecular sensitivity required to detect protein receptors (Fig. 1). With respect to nuclear medicine and optical imaging, there are vast differences in depth sensitivity, instrumentation, and image reconstruction; however, there are substantial similarities as well. Since both provide the ability to detect nanomolar concentrations of imaging agents, all of the image-analysis and kinetic-modeling methods discussed in this review article generally apply to both modalities.

In cancer diagnosis, after initial studies of antibody-based cell-surface receptor imaging in the 1970s (Goldenberg *et al.*, 1978; Mach *et al.*, 1974), the imaging of glucose metabolism with ^{18}F -fluorodeoxyglucose (^{18}F -FDG) positron emission tomography (PET) took over as the standard molecular-imaging approach (Fletcher *et al.*, 2008). Though effective in many cases, ^{18}F -FDG PET has its limitations: (1) increased glucose metabolism is not obvious in all cancer types, with some tumors demonstrating heightened metabolism without contrast on ^{18}F -FDG-PET (Hicks, 2004); (2) increased glucose metabolism is typically confined to aggressive late-stage cancers and may not be as effective as an early indicator of disease (Hicks, 2004); and (3) certain benign lesions are also known to present with heightened glucose metabolism resulting in false-positives (Strauss, 1996). In light of these limitations and the known distinctiveness of cell-surface receptor phenotypes for cancer cells vs. healthy cells (Rettig and Old, 1989), recent developments in molecular imaging have sparked a revival of cell-surface-antigen-targeted imaging for diagnosing cancer (Boerman and Oyen, 2011). For example, in molecular-imaging-guided surgery, a folate-receptor-targeted fluorescent imaging agent was imaged in a landmark study in the Netherlands to improve the identification of ovarian cancer during resection (van Dam *et al.*, 2011). Similarly, for guiding personalized therapy, recent studies in patients with metastatic breast cancer have explored the relationship between pre-therapy expression levels of human epidermal growth factor receptor 2 (HER2) and the response of patients to a HER2-targeted therapy (Mortimer *et al.*, 2014).

Despite recent advances in molecular imaging, there remain many obstacles to realizing the full potential of receptor identification in cancer management. Currently, ^{18}F -FDG PET continues to be the only clinical molecular imaging approach that is widely used for cancer diagnosis/screening (James and Gambhir, 2012), and there has only been one molecular imaging-guided cancer surgery study in humans to date (van Dam *et al.*, 2011). Furthermore, the failure rate for clinical trials of new drugs remains astronomically high, ~95% (DiMasi *et al.*, 2003), even for targeted therapeutics with apriori molecular-imaging guidance (Scott *et al.*, 2012). While the reasons for these apparent shortcomings are debatable and multifaceted, there is a growing recognition that a major problem is the quantitative limitations of conventional imaging approaches often employed for molecular diagnosis and for guiding cancer therapy (Tomasi *et al.*, 2012).

The features that characterize the ideal molecular imaging approach will vary based on each application. For cancer diagnosis and surgical guidance, it may be sufficient to simply delineate between cancerous and healthy tissues, whereas for guiding targeted therapeutics, it may be advantageous to quantify the concentration of drug-targetable receptors. In either case, the signals displayed in a molecular image should ideally be proportional to the concentration of cell-surface receptors. This is challenging considering various nonspecific (non-molecular) factors that can alter the distribution of an exogenous contrast agent, including high physiological variability within and amongst tumors in terms of vascularity, vascular permeability, interstitial pressure, blood flow, etc (Jain, 1990a, b, 2001). In this review article, the history of quantitative cell-surface-receptor molecular imaging is presented, with a particular focus on the quantitative limitations of conventional approaches and potential solutions to mitigate some of these shortcomings, including kinetic modeling and “paired-agent” techniques.

2. Limitations of conventional receptor imaging

The most common approach for imaging cell-surface receptor distribution *in vivo* is the “inject, wait, and image” approach. Here a targeted imaging agent is injected systemically and yields an image of the agent’s retention in the patient after sufficient time has elapsed for unbound concentrations of the agent to be “washed out” of the tissues, ideally leaving only specifically bound agent (Weissleder and Mahmood, 2001). Studies that have employed this approach for imaging cell-surface receptor concentrations in preclinical models and clinical cancer cases now number in the thousands, dating back to the 1970s (Goldenberg *et al.*, 1978; Mach *et al.*, 1974), and have been surveyed in several review articles (Schottelius and Wester, 2009; Yang *et al.*, 2006; Weissleder, 2006; Gambhir, 2002; Van Den Bossche and Van de Wiele, 2004; Ntziachristos *et al.*, 2005; Weissleder, 2002; Leblond *et al.*, 2010; Kaur *et al.*, 2012). With over four decades of studies showcasing the potential benefits of receptor imaging for early diagnosis, for surgical guidance, and for guiding cancer therapies, a critical question to ponder is: why has receptor imaging *not* been adopted to a greater extent by oncologists?

Certainly, the onerous and expensive path for diagnostic agents to become approved for human use is a significant impediment for the clinical adoption of receptor imaging (Choi and Frangioni, 2010; Gioux *et al.*, 2010; Sevick-Muraca, 2012; Sevick-Muraca *et al.*, 2013;

Weissleder, 2006). However, there are more fundamental problems associated with the imaging of cancer-related cell-surface receptors. Most importantly, perhaps, is the high risk of discordance between the measured uptake of an imaging agent and the true concentration of cell-surface receptors. In other words, there are a number of physiological and technological factors that significantly obfuscate the relationship between the signal measured from a targeted imaging agent and its true level of binding to a targeted receptor (Prabhakar *et al.*, 2013). In the case of systemically administered imaging agents – *i.e.*, agents injected into the blood stream – these obfuscating factors can include, but are not limited to, blood flow (Fang *et al.*, 2011), vascular permeability (Jain, 2013; Maeda *et al.*, 2000), extent of vascularization [hypovascular or hypervascular] (Allen and Cullis, 2004), efficacy of lymphatic drainage (Seymour, 1992), cellular internalization of the agent (Bartlett *et al.*, 2007), metabolism of the imaging agent and therefore the potential (at least in nuclear medicine) for metabolites to preferentially accumulate in tumors that exhibit enhanced permeability and retention (Lammertsma, 2002; Maeda, 2001), nonspecific chemical binding (Mintun *et al.*, 1988), spatial diffusion (Wilks *et al.*, 2014), binding-site barriers (Thurber *et al.*, 2008), blood/interstitial pressure (Jain, 1990a, b), and the pharmacokinetics of the agent in the blood [*e.g.*, excretion rate] (Wu and Yazaki, 2000). Many of these factors can be amplified in cancers, and worse, physiological heterogeneities within and amongst tumors can lead to substantial variability in these factors, making the imaging of cell-surface receptors in tumors particularly problematic (Brown and Giaccia, 1998; Brown *et al.*, 2001; Heneweer *et al.*, 2011). In particular, the heightened uptake of “foreign substances” in many tumors compared to normal tissue, now coined the “enhanced permeability and retention (EPR)” effect (Maeda *et al.*, 2000), was originally observed back in the 1930s (Duran-Reynolds, 1939), and is now leveraged in many chemotherapies (Maeda, 2001). For example, increased/preferential uptake of indocyanine green (an untargeted fluorescent agent) was observed in tumors compared to healthy tissue at up to 24 h after injection [Fig. 2] (Kosaka *et al.*, 2011), despite relatively rapid plasma clearance (Krieger *et al.*, 2011). While this result may be leveraged for certain applications such as identifying tumors for surgery, it is a significant problem if one aims to relate the uptake of the targeted imaging agent to the true abundance of the receptor for applications such as image-guided drug therapy. This nonspecific uptake and retention is often overlooked, yet it can become the dominant factor for larger imaging agents such as nanoparticle-based agents where both specific and nonspecific binding/retention can be effectively irreversible and binding rates can far exceed rates of efflux back into the blood (Wittrup *et al.*, 2012). In this scenario, irreversible nonspecific uptake and trapping of large imaging agents may be a dominant effect such that molecular targeting is not likely to enhance their retention; however, many nanoparticle developers continue to functionalize their particles with antibodies and other targeting moieties. In some cases a benefit may be achieved, but proper control studies should be carried out to prove the effect is significant.

It should be noted that additional factors other than delivery and retention can affect the measured uptake of a targeted imaging agent, such as the accuracy and reproducibility of the imaging modality/system used. In response to this challenge, great efforts have been made to quantify signals from more advanced nuclear medicine molecular imaging modalities [PET and SPECT] (Hutton *et al.*, 2011; Kinahan *et al.*, 1998); however, quantification in

fluorescence imaging can be particularly challenging owing to the heterogeneous optical properties of biological tissues, which can greatly affect detected signal levels (Jacques, 2013; Ntziachristos *et al.*, 2005; Hilderbrand and Weissleder, 2010; Sevick-Muraca, 2012). In addition, owing to the limited penetration depth of optical radiation, the geometry of the detection device with respect to a tissue surface (*e.g.*, angle of detection, working distance, etc.) can also affect signal levels.

In light of the significant effects that tumor physiology can have on the uptake and retention of imaging agents in tissue, there are two straightforward, non-exclusive approaches for quantifying receptor concentrations: 1) develop tracers that are less affected by these effects, and 2) develop imaging analysis approaches that can account for these effects and thereby extract receptor concentrations. Extensive efforts have been devoted to developing imaging agents that are less susceptible to nonspecific uptake and delivery effects and there are a number of excellent review articles providing surveys of state-of-the-art agents for targeting cell surface receptors (James and Gambhir, 2012, 2010; Gao *et al.*, 2004; Bai and Bornhop, 2012; Kobayashi and Choyke, 2011; Luo *et al.*, 2011; Tolmachev *et al.*, 2010a; Wu and Senter, 2005; Wu and Yazaki, 2000; Lee *et al.*, 2010). While a discussion of imaging-agent development is outside the scope of this review article, it is important to understand that even the most advanced agents cannot completely circumvent the problems of nonspecific accumulation and delivery variability. The following sections will focus primarily on imaging methodologies and analyses, based on tracer-kinetic and pharmacokinetic modeling, which provide a direct means of quantifying cell-surface receptors (Fig. 3).

3. Quantitative kinetic modeling

The field of quantitative kinetic modeling in cancer molecular imaging stems predominantly from brain PET studies. For a thorough overview of the subject, the reader is referred to a recent comprehensive review article (Gunn *et al.*, 2015). However, owing to the importance of these concepts in this review, a history of *in vivo* kinetic modeling and its progression to cancer imaging is still presented here. The vast majority of kinetic models used in molecular imaging analyses are based on so-called “compartment modeling,” where the problem is simplified by assuming the imaging agent can only be in a set number of physical or chemical “compartments” within a tissue volume. In the early 1980s, landmark papers were published (Mintun *et al.*, 1984; Patlak *et al.*, 1983) presenting simple compartment models that assumed the imaging agent could only be in three compartments: in the blood plasma (C_p), freely associated in the extravascular extracellular (interstitial) space (C_f), or bound specifically to the receptor of interest (C_b) (Fig. 4 & 5a). To model distribution of the imaging agent amongst the compartments in time, first order rate equations were assumed with 4 rate constants, K_1 , k_2 , k_3 , and k_4 ; where the rate of extravasation of the agent (C_p to C_f) is proportional to the concentration in C_p multiplied by the rate constant K_1 , the rate of washout of the agent (C_f to C_p) is proportional to the concentration in C_f multiplied by the rate constant k_2 , the rate of specific binding of the agent to the receptor (C_f to C_b) is proportional to the concentration in C_f multiplied by the rate constant k_3 , and the rate of dissociation of the agent from (C_p to C_f) is proportional to the concentration in C_b multiplied by the rate constant k_4 (Fig 5a).

Two subtle points of the naming convention are worth mentioning: 1) K_1 is the only rate constant that is capitalized to indicate that it is defined as a proportionality associated with the blood plasma concentration of the imaging agent, while all other rate constants are typically defined as proportionalities associated with the voxel concentration of the agent; 2) the “blood” concentration is typically defined as the “blood plasma” concentration. The major components of blood being red blood cells and plasma, the imaging agent is only available to extravasate into the tissue if it is freely associated in the blood plasma and not associated with the red blood cells, and so studies that incorporate a blood draw to analyze the blood concentration of imaging agent typically report on the plasma concentration, C_p . However, if the concentration of agent bound to red blood cells is significant, it should also be measured as it will contribute to the signal measured in the region-of-interest (*ROI*) or

voxel in the image, where $ROI(t) = \eta \sum_i v_i C_i(t)$ with the scaling factor, η , representing the proportionality between the measured signal of an imaging agent (*ROI*) and the true concentration of the imaging agent in the *ROI*, $C_i(t)$ representing the concentration of the imaging agent in the i^{th} compartment (*e.g.* bound concentration, C_b), and v_i being the weighting factors to correct for the fractional volume of the i^{th} compartment in the *ROI*. While the early works on compartment modeling of cell-surface receptor targeted imaging agents focused on the analysis of brain tissue and not cancer, they represent the first imaging approaches capable of estimating cell-surface receptor concentrations *in vivo*, and provide an excellent lead-in to the imaging of receptor concentrations in cancer, which is a far less mature field. In both the Mintun *et al.* and Patlak *et al.* papers, the authors recognized the confounding impact that blood flow, nonspecific binding, and vascular permeability – amongst other factors summarized in **Section 2** – could have on the accurate prediction of receptor concentrations when measuring the uptake of targeted agents at a single time point. The majority of subsequent kinetic modeling methods have been built upon the compartment models proposed in these early works, which assumed three possible environments for the imaging agent: two physical environments (blood and tissue) and one chemical environment (specific binding to tissue receptors). The imaging agent is assumed to be “free” in the tissue compartment prior to association with, or upon dissociation from (for reversible binding), the bound compartment. This assumes that the receptors of interest are located on cells within the tissue compartment and are therefore not directly accessible to agents in the blood.

These early models represent variations of the “arterial input function” imaging methodology represented in Fig. 3B. The model developed by Mintun *et al.* allows for the possibility of reversible binding (k_4), whereas the model developed by Patlak *et al.* assumes that binding is irreversible. The method proposed by Patlak *et al.*, while requiring arterial blood sampling, is relatively straightforward and is widely used today for imaging agents that are assumed to exhibit irreversible binding. However, agents that target cell-surface receptors often exhibit reversible binding characteristics. Patlak and Blasberg followed up their irreversible-binding paper with a more general derivation allowing for reversible binding (Patlak and Blasberg, 1985); yet, even with this new model it is not possible to decouple binding-related parameters (k_3 and k_4) from the blood-tissue rate constants (K_1 and k_2) (a particular problem in cancer imaging as discussed below), nor does the model have

the flexibility to correct for the intravascular contribution to the signal. However these models are insensitive to slow kinetic non-specific compartments. On the other hand, the model proposed by Mintun *et al.* was capable of isolating binding parameters from other kinetic parameters. Unfortunately, the approach was far too complicated to be applied on a wide scale, requiring: (1) arterial blood sampling as an input function, (2) uptake in an ideal “reference tissue” devoid of specific binding to estimate vascular permeability and the non-displaceable fraction of the imaging agent, and (3) subsequent or prior imaging of both blood flow and blood volume using separate radioactive imaging agents, ^{15}O -water (Raichle *et al.*, 1983) and ^{15}O -carbon monoxide (Grubb *et al.*, 1978), respectively. In response to the complexity of the Mintun model, a number of groups have since worked out more simplified approaches to approximate *BP* (see **Section 3.3** for more discussion on the importance of the binding potential parameter), predominantly for neurotransmitter imaging applications (Lammertsma *et al.*, 1996). Some important simplifications that have greatly increased the use of kinetic modeling in molecular imaging include the realization that the arterial input function, which is invasive to measure in nuclear medicine studies, could be derived from serial imaging of the heart or aorta owing to the large blood pool in these regions (Germano *et al.*, 1992), or could be mathematically replaced by the “reference tissue” input function described by Mintun *et al.* that was originally used to estimate vascular permeability (Hume *et al.*, 1992).

3.1 Reference tissue modeling

“Reference tissue” models (Fig. 3C) turn out to be poorly suited for cancer imaging; nevertheless, they warrant some discussion as all of the mathematical models that have been developed for reference-tissue approaches are directly translatable to the “paired-agent” approaches (Fig. 3E), which are described in **Section 4** and are ideal for quantifying receptor concentrations in cancer. Reference-tissue models essentially stemmed from the recognition that if the temporal uptake of an imaging agent in any region of interest is dependent on the following parameters:

- i. arterial input function
- ii. blood-tissue transfer kinetics (K_1 and k_2)
- iii. specific binding and dissociation (k_3 and k_4)

and the uptake of the same imaging agent in a tissue region devoid of targeted receptor (reference tissue) is dependent on only i. and ii., then the reference-tissue uptake may be used to account for i. and ii. in any other tissue region. This, in turn, would allow for an extraction of the binding potential (k_3/k_4) of that region. In other words, the uptake of the imaging agent in a tissue devoid of receptor (reference tissue) can be used as a surrogate of the plasma input function in all other tissues, as long as the ratio of the delivery kinetics (K_1/k_2) of the imaging agent are similar in all tissues (the validity of this assumption will be discussed in the context of tumor imaging below). Hume *et al.* published the original presentation of this approach in 1992 (Hume *et al.*, 1992), but the implications of the approach were not fully appreciated until Lammertsma and Hume (Lammertsma and Hume, 1996) and Logan *et al.* (Logan *et al.*, 1996) published their “simplified” and “graphical” reference tissue models, respectively, which are regularly employed in brain

neurotransmitter PET imaging today. Many modifications of the original reference-tissue model have been explored, with each model requiring its own set of assumptions; however, one assumption that is central to all reference-tissue models is that the dynamics of imaging agent delivery and retention be equivalent between the reference tissue and any other region of interest under analysis (Lammertsma and Hume, 1996). Note that agent delivery and retention are represented by the ratio of rate constants, K_1/k_2 , which in turn are dependent on blood flow, vascular permeability, interstitial pressure, and other factors. As discussed in a recent review on quantitative PET imaging in oncology (Tomasi *et al.*, 2012), this assumption has only been validated in brain-tissue imaging, and it is known that the factors that influence K_1 and k_2 can be highly abnormal in tumors (Jain, 2001). There are a few studies that have employed reference tissue models for cancer imaging (Ardeshirpour *et al.*, 2014; Chernomordik *et al.*, 2010; Hassan *et al.*, 2012; Zielinski *et al.*, 2012; Guo *et al.*, 2012; Zhang *et al.*, 2006; Zhu *et al.*, 2012); however, a recent study from our group demonstrates that tumors can have variable and odd K_1/k_2 ratios that can make it difficult to identify a suitable reference tissue from any healthy tissue (Tichauer *et al.*, 2012a).

3.2 Temporal kinetic analyses

With suitable reference tissue regions being difficult to identify for cancerous tissue (owing to the significant difference between tumor and normal tissues in almost every possible way), most single-imaging-agent receptor-concentration imaging efforts have employed complex kinetic models with numerous fitting parameters similar to the Mintun approach (Mintun *et al.*, 1984). The Mintun approach, in turn, is based on other early two-tissue compartment PET neurotransmitter imaging models that require arterial input functions (Fig. 3B) (Farde *et al.*, 1989; Lammertsma *et al.*, 1996; Sawle *et al.*, 1993; Volkow *et al.*, 1993). A list of kinetic-modeling studies for the imaging of cancer receptors is presented in Table 1. In general, the goal in kinetic modeling is to find a solution with as few parameters as possible while accurately describing as much of the biological behavior as possible. By fitting imaging agent temporal uptake curves, which are relatively featureless, with models that include four or more parameters through nonlinear curve-fitting algorithms, significant parameter covariance can be encountered. Here, covariance refers to models in which changes in two or more parameters can result in similar changes to the model's output (*i.e.* imaging agent-uptake curve shape), thereby reducing the uniqueness of a solution. In addition, models with large numbers of parameters often result in longer computational times, and require relatively accurate initial parameter "guesses" to prevent convergence to local minima, all of which can significantly reduce the accuracy and precision of the model. Software packages for compartment-model fitting often seek to reduce the instability of nonlinear fitting routines (Barrett *et al.*, 1998; Mikolajczyk *et al.*, 1998; Muzic and Cornelius, 2001; Gambhir *et al.*, 1996), and the use of artificial network nodes has been employed with some success to improve convergence to global minima and to speed up computation times (Gambhir *et al.*, 1998). Simplified reference-tissue models (a subcategory of Fig. 3C), introduced by Lammertsma *et al.* (Lammertsma and Hume, 1996), improve conditioning of nonlinear fitting further by reducing the model to three parameters, while linearized and constrained versions of this model have been explored to enhance the noise stability and computational efficiency (Gunn *et al.*, 1997; Hume *et al.*, 1998; Ichise *et al.*, 2003). Graphical models, such as the Patlak (Patlak and Blasberg, 1985) [Fig. 3B model]s

and Logan models (Logan *et al.*, 1996; Logan *et al.*, 1990) [Fig. 3C models], simplify the fitting process further, and as a result, are used in a large number of neurotransmitter imaging studies.

Unfortunately, all of the simplified models in their current form are not readily adaptable to tumor imaging. As mentioned in Section 3.1, reference tissue models are problematic since it is difficult to find an ideal “reference tissue” for all tumors, and the estimates of receptor concentration provided by the Patlak and Logan graphical models are dependent on the dynamics of imaging agent delivery and retention, which often vary substantially within and amongst different tumors (Tichauer *et al.*, 2012a). Moreover, some tumors exhibit substantial nonspecific uptake of foreign substances, which could require addition of a “nonspecific compartment” in the models, thereby increasing the number of fitting parameters depending on whether or not there is rapid equilibrium between free imaging agents and the nonspecific concentrations. In the case of rapid equilibrium, nonspecific retention is often addressed by solving for the “non-displaceable” binding potential, BP_{ND} , which is the product of the true BP and f_{ND} , the fraction of imaging agent in the “free” space that is not associated with the nonspecific compartment [see **Section 4** for further discussion] (Innis *et al.*, 2007).

As a result of these complications, less than 40 articles have been published in the last 25 years that have employed kinetic modeling to estimate cell-surface receptor concentrations in tumors using a single targeted imaging agent, the majority of which are listed in Table 1. This number pales in comparison to the quantity of PET neurotransmitter studies carried out in non-cancerous brain tissue that have been published in the same time period, which number in the thousands. Clearly, a more robust means of imaging receptor concentration in tumors is required in order to achieve acceptance by the wider cancer molecular imaging community, the majority of which continues to rely on the standard “inject-wait-image” protocols that are discussed in Fig. 3A and **Section 2**. **Section 4** reviews the growing field of “paired-agent” imaging that may hold the key for more quantitative imaging of tumor receptors.

3.3 Binding potential

With much of the cancer-imaging world likely being unfamiliar with the kinetic parameter, BP (binding potential), a summary of the parameter is provided here; however, a more detailed discussion of the utility and limitations of BP are presented in a consensus paper (Innis *et al.*, 2007), and in a recent review article (Gunn *et al.*, 2015). In a general sense, the binding potential (BP) can be written as:

$$BP \equiv \frac{k_3}{k_4} = B_{avail} \cdot K_A \quad (1)$$

where B_{avail} represents the concentration of targeted cell-surface receptors *available* for binding and K_A represents the “affinity” of the imaging agent for the receptor [where $K_A = k_{on}/k_{off}$ in the reaction-kinetics literature] (Innis *et al.*, 2007).

In many cases it is possible to approximate K_A from *in vitro* analyses (Annis *et al.*, 2007), and therefore solve Eq. (1) for B_{avail} , yet the majority of articles employing kinetic modeling to estimate receptor concentrations prefer to report BP rather than the B_{avail} . As of August 2014, a PubMed.gov search for the phrase “binding potential” brought up a list of over 1700 publications in the last 20 years, with a relatively consistent increase in the rate of appearance since the early 1990s. There are a number of reasons why BP is considered a preferable parameter to B_{avail} , and why the measurement of BP is proposed for cancer imaging in this review. First, there is evidence that suggests discordance between *in vitro* and *in vivo* measurements of K_A at least in neurotransmitter receptor imaging studies (Laruelle *et al.*, 1994; Robertson *et al.*, 1991), which would suggest that environmental factors can influence the affinity of an imaging agent for its targeted receptor. Since tumor environments tend to be particularly abnormal and variable, the *in vitro* and *in vivo* affinities of a given imaging agent should be compared in extensive studies by varying the occupancy of the receptor with the imaging agent (Laruelle *et al.*, 1993) before attempting to convert *in vivo* images of BP to maps of receptor concentration. A second, more important reason for reporting BP is that it may be more informative for studies of natural ligands or drug binding than the more-difficult-to-quantify receptor concentration. For instance, if BP is measured using an imaging agent analog of a targeted therapeutic or natural ligand, then, as a unitless parameter, that BP could be used directly to estimate the proportion of drug/ligand that will bind to target receptors given a known drug dose or ligand concentration. More specifically, if the concentration of a drug in a tissue is represented by C ($C = C_f + C_b$), which is measurable by conventional molecular imaging if signal can be converted to imaging-agent concentration and the blood concentration of the agent is negligible, then the amount of bound drug could be estimated by the product: $CBP/(1+BP)$ (Mintun *et al.*, 1984).

As a final note, there are many competing approaches for estimating BP that tend to result in one of three different *in vivo* manifestations of the parameter – a non-displaceable BP (BP_{ND}), a “free” BP (BP_F), and a plasma BP (BP_P) – each of which is only proportional to *in vitro* BP (subscript free). A full discussion of the specifics of each BP definition can be found elsewhere (Innis *et al.*, 2007; Gunn *et al.*, 2015). Here, the important definition is BP_{ND} , which results from reference-tissue and paired-agent kinetic analyses and is proportional to the *in vitro* BP multiplied by f_{avail} and f_{ND} , where f_{ND} is the fraction of free imaging agent in the non-displaceable compartment and f_{avail} is the fraction of receptors available for binding *in vivo* compared to *in vitro*.

4. Paired-imaging-agent approaches

Instead of employing complex kinetic models to account for the variable delivery and retention of imaging agents in tumors (**Section 3**), in the 1950s, the group of David Pressman at Roswell Park Memorial Institute took a much more direct approach. Realizing that antibody uptake in tumors could be skewed by significant nonspecific background (Duran-Reynolds, 1939), the group proposed the use of a second, untargeted imaging agent to be administered alongside the targeted antibody. The uptake of the untargeted agent could then be used as an estimate of the extent of nonspecific uptake. The group coined this ingenious approach of estimating specific binding in tumors as *paired-labeling* (Pressman *et al.*, 1957), which has since been referred to as *ratiometric* (Liu *et al.*, 2009; Wang *et al.*,

2012; Wang *et al.*, 2014b) or *dual-probe/reporter/tracer* (Baeten *et al.*, 2009; Pogue *et al.*, 2010; Tichauer *et al.*, 2012c) imaging. In this review article, we propose the use of *paired-agent* imaging to represent all approaches that employ an untargeted imaging agent to account for nonspecific (non-molecular) aspects of a targeted imaging agent's delivery and retention. As an example of the utility of such an approach, one can imagine a scenario where a targeted imaging agent is preferentially retained in a tumor compared to healthy tissue. Conventionally, such a finding would be taken to mean that the targeted agent was binding to the specific cancer receptor it was targeted to. However, using the paired-agent approach, if the untargeted agent is also preferentially retained in the tumor compared to healthy tissue, one could infer that the preferential tumor uptake of the "targeted" agent is due, at least in part, to nonspecific (non-molecular) mechanisms, and that the extent of specific binding to cancer receptors is ambiguous. Paired-agent approaches have the power to identify imaging-agent retention attributable to specific vs. nonspecific binding by the extent to which targeted agent retention is higher than untargeted agent retention in any tissue (Fig. 5 & 6).

The original paired-agent approach was rather involved, entailing the injection of ^{131}I -labeled antiserum antibody and ^{133}I -labeled normal serum antibody with subsequent perfusion of dissected tissues in 1-gram sections for placement in a scintillator well. Since the mean gamma radiation emission energies of the two iodine isotopes were significantly different (360 keV and 530 keV, respectively), signal emissions from each could be separated by a two-channel scintillation spectrometer. Crosstalk between channels was problematic and required a form of normalization to scintillation measurements on fractions of the injected solution prior to injection and at the time of tissue imaging (Pressman *et al.*, 1957). In the years following its initial proposal, paired-agent approaches were adapted for *in vivo* autoradiography (Blau *et al.*, 1958), highlighted in *Nature* in 1962 to quantify chemical differences between antibody fragments (Roholt *et al.*, 1962), and later applied to tissue sections and cell smears (Tanigaki *et al.*, 1967). In the late 1960s and early 1970s, the approach was picked up by the group of Dr. Frank J. Dixon at the Scripps Clinic and Research Foundation to quantify immunogenic activity of antigens (McConahey *et al.*, 1968; McPhaul and Dixon, 1970; Wilson and Dixon, 1971; Wilson *et al.*, 1971); yet only a few groups other than Pressman's applied the approach to cancer receptor analyses (Boone *et al.*, 1973a; Boone *et al.*, 1973b; Duthu and de Vaux Saint-Cyr, 1975; Sears and Wilson, 1981; Chatal *et al.*, 1983; Buchegger *et al.*, 1983; Kurth *et al.*, 1993; Behnke *et al.*, 1988; Matzku *et al.*, 1987). It was not until the mid-1980s that the approach was adopted as regular practice for tumor-receptor imaging by the labs of Dr. Darrel D. Bigner and then Dr. Michael R. Zalutsky at Duke University who have conducted the vast majority of paired-agent studies up to the present, producing more than 60 publications using the method, a selection of which are cited here (Bourdon *et al.*, 1984; Wikstrand *et al.*, 1986; Blasberg *et al.*, 1987; Zalutsky and Narula, 1987; Garg *et al.*, 1992; Reist *et al.*, 1995; Reist *et al.*, 1997; Wikstrand *et al.*, 1997; Foulon *et al.*, 2000; Pruszynski *et al.*, 2014). Outside of the substantial work carried out at Duke University with paired-agent approaches, few other groups have picked up on the methodology for nuclear medicine tumor imaging (Demignot *et al.*, 1990; Sung *et al.*, 1990; Gadina *et al.*, 1991; Khawli *et al.*, 1996; Repetto-Llamazares *et al.*, 2014; Shockley *et al.*, 1992; Stein *et al.*, 2001; Stein *et al.*, 2003; Tolmachev *et al.*,

2010b; Yokota *et al.*, 1993; Terwisscha van Scheltinga *et al.*, 2014). Almost certainly, the limited use of paired-agent approaches is attributable to complexities in carrying out the methodology. First, it involves higher radiation dose because administration of an untargeted radioactive agent in addition to the targeted radioactive agent is required. Second, it can be difficult to accurately resolve signal from targeted and untargeted agents even with advanced gamma cameras owing to crosstalk between gamma emission energy distributions (El Fakhri *et al.*, 2001). Third, it is not possible to resolve signal from more than one species of agent using the more advanced nuclear medicine modality, PET, restricting *in vivo* paired-agent receptor imaging to SPECT systems.

In order to mitigate problems associated with signal crosstalk, a number of groups have preferred to compare targeted-agent uptake in one set of tumor-bearing animals with untargeted-agent uptake in a second, independent set of tumor-bearing animals (Chattopadhyay *et al.*, 2012; Goldenberg *et al.*, 1974; Green *et al.*, 2014; McLarty *et al.*, 2009; Nagengast *et al.*, 2007; Otsuji *et al.*, 1992). While this approach is not adaptable to the clinic, it demonstrates specific uptake for the testing of new drugs or imaging agents. McLarty *et al.* have demonstrated that the ratio of targeted to untargeted agent uptake correlates relatively well with differences in receptor concentration in various tumor lines (McLarty *et al.*, 2009). However, by not injecting both agents into the same animal, the untargeted agent cannot be used to correct for tissue heterogeneity and inter-subject variability and subtle differences in blood plasma kinetics between targeted agents may be less obvious owing to animal-to-animal variability.

As an aside, the use of antibodies by McLarty *et al.* warrants further discussion as antibodies are often considered to be irreversible binding agents since they internalize and become trapped inside cells upon binding to cell-surface receptors at rates that exceed dissociation (Mattes *et al.*, 1994). Under such conditions, there is modeling and data to support the hypothesis that if the tissue concentration of the antibody-based imaging agent is at sub-receptor-saturation levels, all agent taken up by the tissue should be internalized regardless of receptor density (Thurber and Weissleder, 2011b, a). It follows from this hypothesis that receptor density would not be estimable under such conditions even with normalization by an untargeted control imaging agent; however, if a saturating dose is used (McLarty *et al.*, 2009; Thurber and Weissleder, 2011b, a), then the signal can correspond to receptor concentration since excess unbound antibody is able to wash out of the tissue. While the hypothesis that antibody binding is irreversible works well to explain the underestimation of high-receptor-expressing tumor lines in McLarty *et al.*, it is based on the assumption that k_3 is much larger than k_2 . If this were not the case, then kinetic normalization of a targeted imaging agent by an untargeted agent would still allow one to estimate receptor concentration in sub-saturation doses, as long as the model accounts for the fact that antibody binding is irreversible. Interestingly, recent results exploring EGFR concentration with smaller, reversible binding peptide-based imaging agents demonstrated very similar apparent underestimations for A431 xenografts (Tichauer *et al.*, 2012c) as observed by McLarty *et al.* This suggests that these measurements may not be underestimations in EGFR, but rather accurate estimates of the “available” EGFR in an *in vivo* environment. To support this alternative hypothesis, it was recently determined that the proportion of EGFR

available for binding *in vivo* for A431 is significantly lower than the measurement of EGFR *in vitro* (Samkoe *et al.*, 2014), by the same factor observed in McLarty *et al.* Further studies are needed to fully characterize binding conditions of antibodies and whether they can be used effectively in paired-agent imaging.

A more recent approach to minimize signal crosstalk and radioactive dose in paired-agent methods has been to employ the approach with the optical imaging modality. For certain applications, optical imaging is ideally suited for paired-agent approaches: it avoids the use of ionizing radiation and can allow for fast and sensitive measures of the uptake of multiple imaging agents in biological tissue, as long as the light emission wavelengths and/or absorption spectra of each imaging agent are significantly different. However, with the relatively recent development of more advanced optical imaging agents and imaging systems, paired-agent approaches were not adopted in the biomedical optics field until the late 2000s when three groups unearthed the approach for various applications, almost simultaneously (Baeten *et al.*, 2009; Liu *et al.*, 2009; Pogue *et al.*, 2010) [Fig. 6]. Baeten *et al.* observed that activatable protease-sensing fluorescent imaging agents only correlated with expected levels of protease if delivery variability was accounted for by normalizing activatable imaging-agent signals by an internal blood-pool (nonspecific) imaging agent (Baeten *et al.*, 2009). In the context of 3D optical-sectioning microscopy, Liu *et al.* demonstrated that nonspecific background signals, from unbound concentrations of a topically administered targeted imaging agent, could be mitigated through normalization with an untargeted agent (Liu *et al.*, 2009). Finally, Pogue *et al.* introduced a kinetic model that was employed to estimate the binding rate k_3 for an epidermal growth factor (EGF)-targeted imaging agent in a mouse xenograft model (Pogue *et al.*, 2010). This compartment model based approach with two paired imaging agents provides the needed reference to accurately fit data with model-based methods for the molecular binding parameters.

4.1 Paired-agent kinetic modeling

Paired-agent kinetic models had been developed for brain imaging in the late 1980s by Blasberg *et al.* (Blasberg *et al.*, 1987) and Huang *et al.* (Huang *et al.*, 1989); however, neither of these early methods caught on, likely owing to their complexity. Both techniques required plasma input function measurements of the targeted and untargeted imaging agents, and the Huang *et al.* approach involved injection of a high-affinity binding agent in succession with a low-affinity binding agent (since this study was carried out with PET instrumentation, signal from different imaging agents could not be resolved at the same time). It wasn't until recently that it was realized that the highly developed *reference tissue* models developed for neurotransmitter studies in PET (**Section 3.1**) could be translated to *paired-agent* studies in tumors – to directly measure BP as a marker of receptor concentration – if the plasma-input functions of a targeted and untargeted pair of agents could be assumed to be identical (Tichauer *et al.*, 2012c). With the availability of robust commercial fluorescence imaging systems that have been optimized to image signals from at least two fluorescent markers in rapid succession (Keereweer *et al.*, 2012; Nakayama *et al.*, 2011), it is straightforward to quantify targeted receptor concentrations in tumors with a paired-agent approach. Already, such quantitative molecular imaging approaches have been utilized for various applications such as measuring intravascular marker concentrations

(Tichauer *et al.*, 2014a), for imaging of orthotopic tumors via MRI-guided fluorescence tomography (Davis *et al.*, 2013), for surgical guidance (Sinha *et al.*, 2015), and for estimating the extent of metastatic burden in lymph nodes [Fig. 6d] (Tichauer *et al.*, 2014c). Validation in multiple tumor lines is an essential part of validating these methods, and Samkoe *et al.* (Samkoe *et al.*, 2014) have shown that this is possible.

Advancing this field is still complex, because it requires careful selection and or synthesis of optimal targeted/untargeted imaging agent pairs. As mentioned, targeted and untargeted agents need to have similar plasma input functions for the reference tissue-based models to work. This needs to be validated with blood studies, estimated by image-based means (Elliott *et al.*, 2014), or with pulse-dye-densitometry studies (Elliott *et al.*, 2012). Alternatively, it is also possible to account for differences in plasma input function by directly measuring both input functions through blood sampling or image-derived means, or by using a correction based on agent kinetics in tissues devoid of targeted receptor (a deconvolution approach described recently) without actually measuring the plasma kinetics (Tichauer *et al.*, 2014b). A second characteristic of an ideal targeted/untargeted agent pair is that the efficiency of agent delivery and retention (quantified by the ratio K_1/k_2) must be nearly equivalent between the agents within the same tissues (Lammertsma and Hume, 1996). Furthermore, K_1 and k_2 must be substantial enough to provide ample uptake and washout of both targeted and untargeted imaging agents so that differences in binding between the two can be observed. Since these parameters rely on blood flow, vascular permeability, and interstitial pressure; as long as the targeted and untargeted agents are of similar size, geometry, and chemistry (e.g. polarity), such an assumption should hold (Tichauer *et al.*, 2014b), though it should be noted that the FDA-approved untargeted optical imaging agents, fluorescein and indocyanine green, bind readily to proteins in the blood plasma, predominantly albumin, which significantly alters their effective molecular characteristics *in vivo*. Two additional assumptions apply specifically to fluorescence-based paired-agent imaging: 1) There is negligible photobleaching observed over the course of an imaging protocol, or if photobleaching is unavoidable, that the magnitude of bleaching is roughly the same for both the targeted and untargeted agents. 2) The absorption/scattering characteristics, and the average trajectory of the excitation and emission photons, are similar when imaging both the targeted and untargeted agents. Monte Carlo simulations have established that this is an adequate assumption for IRDye-800CW and IRDye-700DX imaged on a LI-COR Pearl System (Kanick *et al.*, 2014); however, such simulations should be repeated for different imaging systems and fluorophore combinations. Finally, recent studies have utilized multiplexed surface enhanced Raman scattering (SERS) nanoparticles that do not photobleach. More importantly, these agents can all be excited at a single illumination wavelength, and all emit within a similar wavelength band (Wang *et al.*, 2014a; Wang *et al.*, 2014b; Zavaleta *et al.*, 2013). The two assumptions mentioned above are therefore both true for this new class of optical imaging agents. Furthermore, these glass-encapsulated gold-core nanoparticles (~120 nm in diameter) are largely identical in terms of size and surface chemistry, and therefore should exhibit similar delivery and retention characteristics in tissue. Recent studies with topically applied SERS NPs conjugated to targeted monoclonal antibodies and isotype-control antibodies (untargeted) have shown that the nonspecific behavior of these targeted and untargeted NPs is virtually identical (Wang *et*

al., 2014a; Wang *et al.*, 2014b). The unique spectral “fingerprint” of SERS NPs offer exquisite signal-to-background properties (Kircher *et al.*, 2012) and the potential to simultaneously image a large multiplexed panel of biomarker targets with laser illumination at a single wavelength (Zavaleta *et al.*, 2008; Zavaleta *et al.*, 2013; Zavaleta *et al.*, 2009), which will be advantageous for identifying and stratifying tumors with greater accuracy in light of the known variability in molecular phenotypes between tumors and even within a single tumor over space and time (Gerlinger *et al.*, 2012). It should be noted, that while these SERS NP imaging agents have demonstrated utility for tissue staining, even paired-agent kinetic modeling may not be sufficient for these and many other targeted/untargeted large imaging-agent pairs owing to high specific and nonspecific tissue uptake coupled with low k_2 rates (tissue release of the imaging agents) (Wittrup *et al.*, 2012). Thus, for systemically delivered imaging agents, paired-agent kinetic modeling will likely only be effective for smaller protein, peptide, and small molecule based agents (rather than nanoparticles) that exhibit appreciable k_2 washout.

Another key point in paired-agent kinetic modeling is the relationship between imaging-agent concentration and the measured signal from the agent. In dual-isotope SPECT, great efforts have been made to quantify respective concentrations of at least two isotopes in biological tissue; however, in optical imaging, the quantification of imaging-agent concentrations is considerably more difficult owing to high levels of light scattering in tissue and the effect of heterogeneous optical properties (Ntziachristos *et al.*, 2003; Frangioni, 2003; Leblond *et al.*, 2010). It is important to note, however, that paired-agent imaging strategies do not require absolute quantification of imaging agent concentrations since the signal from the untargeted agent acts to normalize the signal from the targeted agent. For example, in the ratiometric imaging approach, it is assumed that the signal ratio between targeted and untargeted agents is largely independent of many of the nonspecific effects that are common to all imaging agents and imaging channels (Wang *et al.*, 2012; Wang *et al.*, 2014a; Wang *et al.*, 2014b; Liu *et al.*, 2009).

Note that the measured signal of any one fluorophore is reliant on a number of properties specific to that particular fluorophore, including fluorophore quantum efficiency, optical properties of the tissue, and the detection efficiency of the imaging system at the fluorophore’s emission wavelength. A tissue-specific means of normalizing targeted and untargeted imaging agent signals is necessary in certain cases. Such approaches have included a “reference tissue” normalization approach (assuming concentrations of both agents in a tissue devoid of binding should be equivalent) (Tichauer *et al.*, 2012c), a pixel-based normalization approach (assuming concentration of both agents are equivalent at very early time points after injection in all tissues) (Kanick *et al.*, 2014), and spectral imaging approaches to directly account for tissue optical property heterogeneities (Valdes *et al.*, 2012). It should be noted that autofluorescence background, if significant, must be removed from images prior to the use of any normalization approach. In kinetic modeling, it may be possible to simply subtract off a pre-injection background-fluorescence image for both agent-imaging channels; however, spectral decomposition approaches also offer an accurate means of autofluorescence removal, and do not require pre-injection imaging (Davis *et al.*, 2008). Further to the point, spectral removal of autofluorescence is particularly enhanced

with the emergence of new SERS NP contrast agents that have distinct spectral signatures that can easily be separated from autofluorescence (Kircher *et al.*, 2012; Zavaleta *et al.*, 2008).

Section 5: Conclusions

With the recent application of robust kinetic-modeling techniques and paired-agent methods, in addition to optimized multiple-imaging-agent imaging technologies in both optics and nuclear medicine, preclinical and clinical methods are finally available to accurately quantify cell-surface receptor concentrations in cancerous lesions through noninvasive and relatively straightforward means. The methods are now available to exploit these assays to, for example, guide personalized medicine or optimize surgical resection procedures in human therapy, or to assist in the development and discovery of new drugs in pre-clinical work. Customization of imaging tools to display BP or receptor concentration values directly may be the next technological advance that will help translate these methods into wider practice.

Acknowledgments

This work was sponsored by the US National Institutes of Health research grants R21 EB015016, R01 CA109558, and R01 CA167413.

References

- Molecular Imaging: Principles and Practice. Shelton, CT: People's Medical Publishing House (PMPH) - USA; 2010.
- Allen TM, Cullis PR. Drug delivery systems: entering the mainstream. *Science*. 2004; 303:1818–22. [PubMed: 15031496]
- Annis DA, Shipps GW Jr, Deng Y, Popovici-Muller J, Siddiqui MA, Curran PJ, Gowen M, Windsor WT. Method for quantitative protein-ligand affinity measurements in compound mixtures. *Analytical chemistry*. 2007; 79:4538–42. [PubMed: 17500537]
- Ardeshirpour Y, Hassan M, Zielinski R, Horton JA, Capala J, Gandjbakhche AH, Chernomordik V. In Vivo Assessment of HER2 Receptor Density in HER2-positive Tumors by Near-infrared Imaging, Using Repeated Injections of the Fluorescent Probe. *Technology in cancer research & treatment*. 2014; 13:427–34. [PubMed: 24000992]
- Baeten J, Haller J, Shih H, Ntziachristos V. In vivo investigation of breast cancer progression by use of an internal control. *Neoplasia*. 2009; 11:220–7. [PubMed: 19242603]
- Bahce I, Smit EF, Lubberink M, van der Veldt AA, Yaqub M, Windhorst AD, Schuit RC, Thunnissen E, Heideman DA, Postmus PE, Lammertsma AA, Hendrikse NH. Development of [(11)C]erlotinib positron emission tomography for in vivo evaluation of EGF receptor mutational status. *Clinical cancer research : an official journal of the American Association for Cancer Research*. 2013; 19:183–93. [PubMed: 23136193]
- Bai M, Bornhop DJ. Recent advances in receptor-targeted fluorescent probes for in vivo cancer imaging. *Current medicinal chemistry*. 2012; 19:4742–58. [PubMed: 22873663]
- Baloch ZW, LiVolsi VA, Asa SL, Rosai J, Merino MJ, Randolph G, Vielh P, DeMay RM, Sidawy MK, Frable WJ. Diagnostic terminology and morphologic criteria for cytologic diagnosis of thyroid lesions: a synopsis of the National Cancer Institute Thyroid Fine-Needle Aspiration State of the Science Conference. *Diagnostic cytopathology*. 2008; 36:425–37. [PubMed: 18478609]
- Barrett PH, Bell BM, Cobelli C, Golde H, Schumitzky A, Vicini P, Foster DM. SAAM II: Simulation, Analysis, and Modeling Software for tracer and pharmacokinetic studies. *Metabolism: clinical and experimental*. 1998; 47:484–92. [PubMed: 9550550]

- Bartlett DW, Su H, Hildebrandt IJ, Weber WA, Davis ME. Impact of tumor-specific targeting on the biodistribution and efficacy of siRNA nanoparticles measured by multimodality in vivo imaging. *Proceedings of the National Academy of Sciences of the United States of America*. 2007; 104:15549–54. [PubMed: 17875985]
- Beattie BJ, Smith-Jones PM, Jhanwar YS, Schoder H, Schmidlein CR, Morris MJ, Zanzonico P, Squire O, Meirelles GS, Finn R, Namavari M, Cai S, Scher HI, Larson SM, Humm JL. Pharmacokinetic assessment of the uptake of 16beta-18F-fluoro-5alpha-dihydrotestosterone (FDHT) in prostate tumors as measured by PET. *Journal of nuclear medicine : official publication, Society of Nuclear Medicine*. 2010; 51:183–92.
- Beer AJ, Grosu AL, Carlsen J, Kolk A, Sarbia M, Stangier I, Watzlowik P, Wester HJ, Haubner R, Schwaiger M. [18F]galacto-RGD positron emission tomography for imaging of alphavbeta3 expression on the neovasculature in patients with squamous cell carcinoma of the head and neck. *Clinical cancer research : an official journal of the American Association for Cancer Research*. 2007; 13:6610–6. [PubMed: 18006761]
- Beer AJ, Haubner R, Goebel M, Luderschmidt S, Spilker ME, Wester HJ, Weber WA, Schwaiger M. Biodistribution and pharmacokinetics of the alphavbeta3-selective tracer 18F-galacto-RGD in cancer patients. *Journal of nuclear medicine : official publication, Society of Nuclear Medicine*. 2005; 46:1333–41.
- Behnke J, Mach JP, Buchegger F, Carrel S, Delaloye B, De Tribolet N. In vivo localisation of radiolabelled monoclonal antibody in human gliomas. *British journal of neurosurgery*. 1988; 2:193–7. [PubMed: 3267303]
- Blasberg RG, Nakagawa H, Bourdon MA, Groothuis DR, Patlak CS, Bigner DD. Regional localization of a glioma-associated antigen defined by monoclonal antibody 81C6 in vivo: kinetics and implications for diagnosis and therapy. *Cancer Res*. 1987; 47:4432–43. [PubMed: 3607773]
- Blau M, Johnson AC, Pressman D. p-Iodobenzoyl groups as a paired label for in vivo protein distribution studies; specific localization of anti-tissue antibodies. *The International journal of applied radiation and isotopes*. 1958; 3:217–25. [PubMed: 13586949]
- Boerman OC, Oyen WJG. Immuno-PET of Cancer: A Revival of Antibody Imaging. *Journal of Nuclear Medicine*. 2011; 52:1171–2. [PubMed: 21764784]
- Boone CW, Church EC, McAllister RM. Testing by the “paired-label” antibody binding technique for feline leukemia virus-induced cell surface antigens (FeLV-CSA) on the surface of human rhabdomyosarcoma cells releasing RD-114 virus. *Virology*. 1973a; 55:157–62. [PubMed: 4353951]
- Boone CW, Gordin F, Kawakami TG. Surface antigens on cat leukemic cells induced by feline leukemia virus: area density and antibody-binding affinity. *Journal of virology*. 1973b; 11:515–9. [PubMed: 4349492]
- Bourdon MA, Coleman RE, Blasberg RG, Groothuis DR, Bigner DD. Monoclonal antibody localization in subcutaneous and intracranial human glioma xenografts: paired-label and imaging analysis. *Anticancer research*. 1984; 4:133–40. [PubMed: 6465851]
- Brannon-Peppas L, Blanchette JO. Nanoparticle and targeted systems for cancer therapy. *Adv Drug Deliver Rev*. 2012; 64:206–12.
- Brown EB, Campbell RB, Tsuzuki Y, Xu L, Carmeliet P, Fukumura D, Jain RK. In vivo measurement of gene expression, angiogenesis and physiological function in tumors using multiphoton laser scanning microscopy. *Nature medicine*. 2001; 7:864–8.
- Brown JM, Giaccia AJ. The unique physiology of solid tumors: opportunities (and problems) for cancer therapy. *Cancer Res*. 1998; 58:1408–16. [PubMed: 9537241]
- Buchegger F, Haskell CM, Schreyer M, Scazziga BR, Randin S, Carrel S, Mach JP. Radiolabeled fragments of monoclonal antibodies against carcinoembryonic antigen for localization of human colon carcinoma grafted into nude mice. *The Journal of experimental medicine*. 1983; 158:413–27. [PubMed: 6886623]
- Buck JR, McKinley ET, Hight MR, Fu A, Tang D, Smith RA, Tantawy MN, Peterson TE, Colvin D, Ansari MS, Baldwin RM, Zhao P, Guleryuz S, Manning HC. Quantitative, preclinical PET of translocator protein expression in glioma using 18F-N-fluoroacetyl-N-(2,5-dimethoxybenzyl)-2-phenoxyaniline. *Journal of nuclear medicine : official publication, Society of Nuclear Medicine*. 2011; 52:107–14.

- Chatal JF, Bourdoiseau M, Fumoleau P, Douillard JY, Kremer M, Curtet C, Le Mevel B. Use of radio-labelled monoclonal antibodies for the scintigraphic detection of human colorectal cancers. *Bulletin du cancer*. 1983; 70:103–7. [PubMed: 6871485]
- Chattopadhyay N, Fonge H, Cai Z, Scollard D, Lechtman E, Done SJ, Pignol JP, Reilly RM. Role of antibody-mediated tumor targeting and route of administration in nanoparticle tumor accumulation in vivo. *Mol Pharm*. 2012; 9:2168–79. [PubMed: 22734589]
- Cheal SM, Punzalan B, Doran MG, Evans MJ, Osborne JR, Lewis JS, Zanzonico P, Larson SM. Pairwise comparison of 89Zr- and 124I-labeled cG250 based on positron emission tomography imaging and nonlinear immunokinetic modeling: in vivo carbonic anhydrase IX receptor binding and internalization in mouse xenografts of clear-cell renal cell carcinoma. *European journal of nuclear medicine and molecular imaging*. 2014; 41:985–94. [PubMed: 24604591]
- Chernomordik V, Hassan M, Lee SB, Zielinski R, Gandjbakhche A, Capala J. Quantitative analysis of Her2 receptor expression in vivo by near-infrared optical imaging. *Molecular imaging*. 2010; 9:192–200. [PubMed: 20643022]
- Choi HS, Frangioni JV. Nanoparticles for biomedical imaging: fundamentals of clinical translation. *Molecular imaging*. 2010; 9:291–310. [PubMed: 21084027]
- Daghighian F, Pentlow KS, Larson SM, Graham MC, DiResta GR, Yeh SD, Macapinlac H, Finn RD, Arbit E, Cheung NK. Development of a method to measure kinetics of radiolabelled monoclonal antibody in human tumour with applications to microdosimetry: positron emission tomography studies of iodine-124 labelled 3F8 monoclonal antibody in glioma. *European journal of nuclear medicine*. 1993; 20:402–9. [PubMed: 8519259]
- Davis SC, Pogue BW, Springett R, Leussler C, Mazurkewitz P, Tuttle SB, Gibbs-Strauss SL, Jiang SS, Dehghani H, Paulsen KD. Magnetic resonance-coupled fluorescence tomography scanner for molecular imaging of tissue. *Review of Scientific Instruments*. 2008:79.
- Davis SC, Samkoe KS, Tichauer KM, Sexton KJ, Gunn JR, Deharvengt SJ, Hasan T, Pogue BW. Dynamic dual-tracer MRI-guided fluorescence tomography to quantify receptor density in vivo. *Proceedings of the National Academy of Sciences of the United States of America*. 2013; 110:9025–30. [PubMed: 23671066]
- de Wiele CV, Boersma H, Dierckx RA, De Spiegeleer B, Van Waarde A, Elsinga PH. Growth Factor/Peptide Receptor Imaging for the Development of Targeted Therapy in Oncology. *Curr Pharm Design*. 2008; 14:3340–7.
- DeMarzo AM, Nelson WG, Isaacs WB, Epstein JI. Pathological and molecular aspects of prostate cancer. *Lancet*. 2003; 361:955–64. [PubMed: 12648986]
- Demignot S, Pimm MV, Baldwin RW. Comparison of biodistribution of 791T/36 monoclonal antibody and its Fab/c fragment in BALB/c mice and nude mice bearing human tumor xenografts. *Cancer Res*. 1990; 50:2936–42. [PubMed: 2334894]
- DiMasi JA, Hansen RW, Grabowski HG. The price of innovation: new estimates of drug development costs. *Journal of health economics*. 2003; 22:151–85. [PubMed: 12606142]
- Dimitrakopoulou-Strauss A, Georgoulas V, Eisenhut M, Herth F, Koukouraki S, Macke HR, Haberkorn U, Strauss LG. Quantitative assessment of SSTR2 expression in patients with non-small cell lung cancer using (68)Ga-DOTATOC PET and comparison with (18)F-FDG PET. *European journal of nuclear medicine and molecular imaging*. 2006; 33:823–30. [PubMed: 16570185]
- Dimitrakopoulou-Strauss A, Seiz M, Tuettenberg J, Schmieder K, Eisenhut M, Haberkorn U, Strauss LG. Pharmacokinetic studies of (6)(8)Ga-labeled Bombesin ((6)(8)Ga-BZH(3)) and F-18 FDG PET in patients with recurrent gliomas and comparison to grading: preliminary results. *Clinical nuclear medicine*. 2011; 36:101–8. [PubMed: 21220970]
- Duran-Reynolds F. Studies on the localization of dyes and foreign proteins in normal and malignant tissues. *Am J Cancer*. 1939; 35:98.
- Duthu A, de Vaux Saint-Cyr C. Neoantigens on cells transformed by SV40. IV.- A quantitative study of antigenic sites in a cell line (TSV5C12) (author's transl). *Annales d'immunologie*. 1975; 126:219–30.
- El Fakhri G, Kijewski MF, Moore SC. Absolute activity quantitation from projections using an analytical approach: Comparison with iterative methods in Tc-99m and I-123 brain SPECT. *Ieee T Nucl Sci*. 2001; 48:768–73.

- Elliott JT, Tichauer KM, Samkoe KS, Gunn JR, Sexton KJ, Pogue BW. Direct Characterization of Arterial Input Functions by Fluorescence Imaging of Exposed Carotid Artery to Facilitate Kinetic Analysis. *Molecular imaging and biology : MIB : the official publication of the Academy of Molecular Imaging*. 2014
- Elliott JT, Wright EA, Tichauer KM, Diop M, Morrison LB, Pogue BW, Lee TY, St Lawrence K. Arterial input function of an optical tracer for dynamic contrast enhanced imaging can be determined from pulse oximetry oxygen saturation measurements. *Physics in medicine and biology*. 2012; 57:8285–95. [PubMed: 23190567]
- Fang J, Nakamura H, Maeda H. The EPR effect: Unique features of tumor blood vessels for drug delivery, factors involved, and limitations and augmentation of the effect. *Adv Drug Deliv Rev*. 2011; 63:136–51. [PubMed: 20441782]
- Farde L, Eriksson L, Blomquist G, Halldin C. Kinetic analysis of central [11C]raclopride binding to D2-dopamine receptors studied by PET--a comparison to the equilibrium analysis. *Journal of cerebral blood flow and metabolism : official journal of the International Society of Cerebral Blood Flow and Metabolism*. 1989; 9:696–708.
- Ferl GZ, Dumont RA, Hildebrandt IJ, Armijo A, Haubner R, Reischl G, Su H, Weber WA, Huang SC. Derivation of a compartmental model for quantifying 64Cu-DOTA-RGD kinetics in tumor-bearing mice. *Journal of nuclear medicine : official publication, Society of Nuclear Medicine*. 2009; 50:250–8.
- Fidler IJ. Tumor heterogeneity and the biology of cancer invasion and metastasis. *Cancer Res*. 1978; 38:2651–60. [PubMed: 354778]
- Fletcher JW, Djulbegovic B, Soares HP, Siegel BA, Lowe VJ, Lyman GH, Coleman RE, Wahl R, Paschold JC, Avril N, Einhorn LH, Suh WW, Samson D, Delbeke D, Gorman M, Shields AF. Recommendations on the use of 18F-FDG PET in oncology. *Journal of nuclear medicine : official publication, Society of Nuclear Medicine*. 2008; 49:480–508.
- Foulon CF, Reist CJ, Bigner DD, Zalutsky MR. Radioiodination via D-amino acid peptide enhances cellular retention and tumor xenograft targeting of an internalizing anti-epidermal growth factor receptor variant III monoclonal antibody. *Cancer Res*. 2000; 60:4453–60. [PubMed: 10969792]
- Frangioni JV. In vivo near-infrared fluorescence imaging. *Current opinion in chemical biology*. 2003; 7:626–34. [PubMed: 14580568]
- Gadina M, Canevari S, Ripamonti M, Mariani M, Colnaghi MI. Preclinical pharmacokinetics and localization studies of the radioiodinated anti-ovarian carcinoma MAb MOv18. *International journal of radiation applications and instrumentation. Part B, Nuclear medicine and biology*. 1991; 18:403–8.
- Gambhir SS. Molecular imaging of cancer with positron emission tomography. *Nat Rev Cancer*. 2002; 2:683–93. [PubMed: 12209157]
- Gambhir SS, Keppenne CL, Banerjee PK, Phelps ME. A new method to estimate parameters of linear compartmental models using artificial neural networks. *Phys Med Biol*. 1998; 43:1659–78. [PubMed: 9651032]
- Gambhir SS, Mahoney DK, Huang SC, Phelps ME. Symbolic interactive modeling package and learning environment (SIMPLE), a new easy method for compartment modeling. *Proc Soc Comput Simul*. 1996:173–86.
- Gao X, Cui Y, Levenson RM, Chung LW, Nie S. In vivo cancer targeting and imaging with semiconductor quantum dots. *Nature biotechnology*. 2004; 22:969–76.
- Garg PK, Garg S, Bigner DD, Zalutsky MR. Localization of fluorine-18-labeled Mel-14 monoclonal antibody F(ab')₂ fragment in a subcutaneous xenograft model. *Cancer Res*. 1992; 52:5054–60. [PubMed: 1516061]
- Gerlinger M, Rowan AJ, Horswell S, Larkin J, Endesfelder D, Gronroos E, Martinez P, Matthews N, Stewart A, Tarpey P, Varela I, Phillimore B, Begum S, McDonald NQ, Butler A, Jones D, Raine K, Latimer C, Santos CR, Nohadani M, Eklund AC, Spencer-Dene B, Clark G, Pickering L, Stamp G, Gore M, Szallasi Z, Downward J, Futreal PA, Swanton C. Intratumor heterogeneity and branched evolution revealed by multiregion sequencing. *The New England journal of medicine*. 2012; 366:883–92. [PubMed: 22397650]

- Germano G, Chen BC, Huang SC, Gambhir SS, Hoffman EJ, Phelps ME. Use of the abdominal aorta for arterial input function determination in hepatic and renal PET studies. *Journal of nuclear medicine : official publication, Society of Nuclear Medicine*. 1992; 33:613–20.
- Gioux S, Choi HS, Frangioni JV. Image-Guided Surgery Using Invisible Near-Infrared Light: Fundamentals of Clinical Translation. *Molecular imaging*. 2010; 9:237–55. [PubMed: 20868625]
- Goldenberg DM, DeLand F, Kim E, Bennett S, Primus FJ, van Nagell JR Jr, Estes N, DeSimone P, Rayburn P. Use of radiolabeled antibodies to carcinoembryonic antigen for the detection and localization of diverse cancers by external photoscanning. *The New England journal of medicine*. 1978; 298:1384–6. [PubMed: 349387]
- Goldenberg DM, Preston DF, Primus FJ, Hansen HJ. Photoscan localization of GW-39 tumors in hamsters using radiolabeled anticarcinoembryonic antigen immunoglobulin G. *Cancer Res*. 1974; 34:1–9. [PubMed: 4809458]
- Green DJ, Orgun NN, Jones JC, Hylarides MD, Pagel JM, Hamlin DK, Wilbur DS, Lin Y, Fisher DR, Kenoyer AL, Frayo SL, Gopal AK, Orozco JJ, Gooley TA, Wood BL, Bensinger WI, Press OW. A preclinical model of CD38-pretargeted radioimmunotherapy for plasma cell malignancies. *Cancer Res*. 2014; 74:1179–89. [PubMed: 24371230]
- Grubb RL Jr, Raichle ME, Higgins CS, Eichling JO. Measurement of regional cerebral blood volume by emission tomography. *Annals of neurology*. 1978; 4:322–8. [PubMed: 727738]
- Gunn RN, Lammertsma AA, Hume SP, Cunningham VJ. Parametric imaging of ligand-receptor binding in PET using a simplified reference region model. *NeuroImage*. 1997; 6:279–87. [PubMed: 9417971]
- Gunn RN, Slifstein M, Searle GE, Price JC. Quantitative imaging of protein targets in the human brain with PET. *Physics in Medicine and Biology*. 2015 in press.
- Guo N, Lang L, Li W, Kiesewetter DO, Gao H, Niu G, Xie Q, Chen X. Quantitative analysis and comparison study of [18F]AIF-NOTA-PRGD2, [18F]FPPRGD2 and [68Ga]Ga-NOTA-PRGD2 using a reference tissue model. *PloS one*. 2012; 7:e37506. [PubMed: 22624041]
- Gurfinkel M, Ke S, Wang W, Li C, Sevick-Muraca EM. Quantifying molecular specificity of alphavbeta3 integrin-targeted optical contrast agents with dynamic optical imaging. *J Biomed Opt*. 2005; 10:034019. [PubMed: 16229663]
- Hamzei N, Samkoe KS, Elliott JT, Holt RW, Gunn JR, Lee TY, Hasan T, Pogue BW, Tichauer K. Comparison of kinetic models for dual-tracer receptor concentration imaging in tumors. *Austin J Biomed Eng*. 2014; 1:9.
- Hassan M, Chernomordik V, Zielinski R, Ardeshirpour Y, Capala J, Gandjbakhche A. In vivo method to monitor changes in HER2 expression using near-infrared fluorescence imaging. *Molecular imaging*. 2012; 11:177–86. [PubMed: 22554482]
- Heneweuer C, Holland JP, Divilov V, Carlin S, Lewis JS. Magnitude of enhanced permeability and retention effect in tumors with different phenotypes: 89Zr-albumin as a model system. *Journal of nuclear medicine : official publication, Society of Nuclear Medicine*. 2011; 52:625–33.
- Henze M, Dimitrakopoulou-Strauss A, Milker-Zabel S, Schuhmacher J, Strauss LG, Doll J, Macke HR, Eisenhut M, Debus J, Haberkorn U. Characterization of 68Ga-DOTA-D-Phe1-Tyr3-octreotide kinetics in patients with meningiomas. *Journal of nuclear medicine : official publication, Society of Nuclear Medicine*. 2005; 46:763–9.
- Hicks RJ. Beyond FDG: novel PET tracers for cancer imaging. *Cancer imaging : the official publication of the International Cancer Imaging Society*. 2004; 4:22–4. [PubMed: 18211857]
- Hilderbrand SA, Weissleder R. Near-infrared fluorescence: application to in vivo molecular imaging. *Current opinion in chemical biology*. 2010; 14:71–9. [PubMed: 19879798]
- Huang SC, Bahn MM, Barrio JR, Hoffman JM, Satyamurthy N, Hawkins RA, Mazziotta JC, Phelps ME. A double-injection technique for in vivo measurement of dopamine D2-receptor density in monkeys with 3-(2'-[18F]fluoroethyl)spiperone and dynamic positron emission tomography. *Journal of cerebral blood flow and metabolism : official journal of the International Society of Cerebral Blood Flow and Metabolism*. 1989; 9:850–8.
- Hume SP, Gunn RN, Jones T. Pharmacological constraints associated with positron emission tomographic scanning of small laboratory animals. *European journal of nuclear medicine*. 1998; 25:173–6. [PubMed: 9473266]

- Hume SP, Myers R, Bloomfield PM, Opacka-Juffry J, Cremer JE, Ahier RG, Luthra SK, Brooks DJ, Lammertsma AA. Quantitation of carbon-11-labeled raclopride in rat striatum using positron emission tomography. *Synapse*. 1992; 12:47–54. [PubMed: 1411963]
- Hutton BF, Buvat I, Beekman FJ. Review and current status of SPECT scatter correction. *Phys Med Biol*. 2011; 56:R85–112. [PubMed: 21701055]
- Ichise M, Liow JS, Lu JQ, Takano A, Model K, Toyama H, Suhara T, Suzuki K, Innis RB, Carson RE. Linearized reference tissue parametric imaging methods: application to [11C]DASB positron emission tomography studies of the serotonin transporter in human brain. *Journal of cerebral blood flow and metabolism : official journal of the International Society of Cerebral Blood Flow and Metabolism*. 2003; 23:1096–112.
- Innis RB, Cunningham VJ, Delforge J, Fujita M, Gjedde A, Gunn RN, Holden J, Houle S, Huang SC, Ichise M, Iida H, Ito H, Kimura Y, Koeppe RA, Knudsen GM, Knuuti J, Lammertsma AA, Laruelle M, Logan J, Maguire RP, Mintun MA, Morris ED, Parsey R, Price JC, Slifstein M, Sossi V, Suhara T, Votaw JR, Wong DF, Carson RE. Consensus nomenclature for in vivo imaging of reversibly binding radioligands. *Journal of cerebral blood flow and metabolism : official journal of the International Society of Cerebral Blood Flow and Metabolism*. 2007; 27:1533–9.
- Jacques SL. Optical properties of biological tissues: a review. *Phys Med Biol*. 2013; 58:R37–61. [PubMed: 23666068]
- Jain RK. Physiological barriers to delivery of monoclonal antibodies and other macromolecules in tumors. *Cancer Res*. 1990a; 50:814s–9s. [PubMed: 2404582]
- Jain RK. Vascular and interstitial barriers to delivery of therapeutic agents in tumors. *Cancer Metastasis Rev*. 1990b; 9:253–66. [PubMed: 2292138]
- Jain RK. Delivery of molecular and cellular medicine to solid tumors. *Adv Drug Deliv Rev*. 2001; 46:149–68. [PubMed: 11259838]
- Jain RK. Normalizing tumor microenvironment to treat cancer: bench to bedside to biomarkers. *Journal of clinical oncology : official journal of the American Society of Clinical Oncology*. 2013; 31:2205–18. [PubMed: 23669226]
- James ML, Gambhir SS. A molecular imaging primer: modalities, imaging agents, and applications. *Physiological reviews*. 2012; 92:897–965. [PubMed: 22535898]
- Kanick SC, Tichauer KM, Gunn JR, Samkoe KS, Pogue BW. Pixel-based absorption-correction for dual-tracer fluorescence imaging of receptor binding. *Biomedical optics express*. 2014; 5:3280–91. [PubMed: 25360349]
- Kaur S, Venktaraman G, Jain M, Senapati S, Garg PK, Batra SK. Recent trends in antibody-based oncologic imaging. *Cancer Lett*. 2012; 315:97–111. [PubMed: 22104729]
- Keereweer S, Mol IM, Vahrmeijer AL, Van Driel PB, Baatenburg de Jong RJ, Kerrebijn JD, Lowik CW. Dual wavelength tumor targeting for detection of hypopharyngeal cancer using near-infrared optical imaging in an animal model. *International journal of cancer. Journal international du cancer*. 2012; 131:1633–40. [PubMed: 22234729]
- Khawli LA, Glasky MS, Alauddin MM, Epstein AL. Improved tumor localization and radioimaging with chemically modified monoclonal antibodies. *Cancer biotherapy & radiopharmaceuticals*. 1996; 11:203–15. [PubMed: 10851539]
- Kinahan PE, Townsend DW, Beyer T, Sashin D. Attenuation correction for a combined 3D PET/CT scanner. *Med Phys*. 1998; 25:2046–53. [PubMed: 9800714]
- Kircher MF, de la Zerda A, Jokerst JV, Zavaleta CL, Kempen PJ, Mitra E, Pitter K, Huang R, Campos C, Habte F, Sinclair R, Brennan CW, Mellinghoff IK, Holland EC, Gambhir SS. A brain tumor molecular imaging strategy using a new triple-modality MRI-photoacoustic-Raman nanoparticle. *Nature medicine*. 2012; 18:829–34.
- Kobayashi H, Choyke PL. Target-cancer-cell-specific activatable fluorescence imaging probes: rational design and in vivo applications. *Acc Chem Res*. 2011; 44:83–90. [PubMed: 21062101]
- Kosaka N, Mitsunaga M, Longmire MR, Choyke PL, Kobayashi H. Near infrared fluorescence-guided real-time endoscopic detection of peritoneal ovarian cancer nodules using intravenously injected indocyanine green. *International journal of cancer. Journal international du cancer*. 2011; 129:1671–7. [PubMed: 21469142]

- Koukouraki S, Strauss LG, Georgoulas V, Eisenhut M, Haberkorn U, Dimitrakopoulou-Strauss A. Comparison of the pharmacokinetics of ⁶⁸Ga-DOTATOC and [¹⁸F]FDG in patients with metastatic neuroendocrine tumours scheduled for ⁹⁰Y-DOTATOC therapy. *European journal of nuclear medicine and molecular imaging*. 2006a; 33:1115–22. [PubMed: 16763820]
- Koukouraki S, Strauss LG, Georgoulas V, Schuhmacher J, Haberkorn U, Karkavitsas N, Dimitrakopoulou-Strauss A. Evaluation of the pharmacokinetics of ⁶⁸Ga-DOTATOC in patients with metastatic neuroendocrine tumours scheduled for ⁹⁰Y-DOTATOC therapy. *European journal of nuclear medicine and molecular imaging*. 2006b; 33:460–6. [PubMed: 16437218]
- Krieger PM, Tamandl D, Herberger B, Faybik P, Fleischmann E, Maresch J, Gruenberger T. Evaluation of chemotherapy-associated liver injury in patients with colorectal cancer liver metastases using indocyanine green clearance testing. *Annals of surgical oncology*. 2011; 18:1644–50. [PubMed: 21207168]
- Kurth M, Pelegrin A, Rose K, Offord RE, Pochon S, Mach JP, Buchegger F. Site-specific conjugation of a radioiodinated phenethylamine derivative to a monoclonal antibody results in increased radioactivity localization in tumor. *J Med Chem*. 1993; 36:1255–61. [PubMed: 8487262]
- Lammertsma AA. Radioligand studies: imaging and quantitative analysis. *European neuropsychopharmacology : the journal of the European College of Neuropsychopharmacology*. 2002; 12:513–6. [PubMed: 12468014]
- Lammertsma AA, Bench CJ, Hume SP, Osman S, Gunn K, Brooks DJ, Frackowiak RS. Comparison of methods for analysis of clinical [¹¹C]raclopride studies. *Journal of cerebral blood flow and metabolism : official journal of the International Society of Cerebral Blood Flow and Metabolism*. 1996; 16:42–52.
- Lammertsma AA, Hume SP. Simplified reference tissue model for PET receptor studies. *NeuroImage*. 1996; 4:153–8. [PubMed: 9345505]
- Laruelle M, Abi-Dargham A, al-Tikriti MS, Baldwin RM, Zea-Ponce Y, Zoghbi SS, Charney DS, Hoffer PB, Innis RB. SPECT quantification of [¹²³I]iomazenil binding to benzodiazepine receptors in nonhuman primates: II. Equilibrium analysis of constant infusion experiments and correlation with in vitro parameters. *Journal of cerebral blood flow and metabolism : official journal of the International Society of Cerebral Blood Flow and Metabolism*. 1994; 14:453–65.
- Laruelle M, Abi-Dargham A, Rattner Z, al-Tikriti MS, Zea-Ponce Y, Zoghbi SS, Charney DS, Price J, Frost JJ, Hoffer PB, et al. Single photon emission tomography measurement of benzodiazepine receptor number and affinity in primate brain: a constant infusion paradigm with [¹²³I]iomazenil. *European journal of pharmacology*. 1993; 230:119–23. [PubMed: 8381354]
- Leblond F, Davis SC, Valdes PA, Pogue BW. Pre-clinical whole-body fluorescence imaging: Review of instruments, methods and applications. *Journal of photochemistry and photobiology. B, Biology*. 2010; 98:77–94.
- Lee S, Xie J, Chen X. Peptides and peptide hormones for molecular imaging and disease diagnosis. *Chemical reviews*. 2010; 110:3087–111. [PubMed: 20225899]
- Leigh SY, Chen Y, Liu JT. Modulated-alignment dual-axis (MAD) confocal microscopy for deep optical sectioning in tissues. *Biomedical optics express*. 2014; 5:1709–20. [PubMed: 24940534]
- Liu JT, Helms MW, Mandella MJ, Crawford JM, Kino GS, Contag CH. Quantifying cell-surface biomarker expression in thick tissues with ratiometric three-dimensional microscopy. *Biophys J*. 2009; 96:2405–14. [PubMed: 19289065]
- Liu JT, Meza D, Sanai N. Trends in fluorescence image-guided surgery for gliomas. *Neurosurgery*. 2014; 75:61–71. [PubMed: 24618801]
- Logan J, Fowler JS, Volkow ND, Wang GJ, Ding YS, Alexoff DL. Distribution volume ratios without blood sampling from graphical analysis of PET data. *Journal of cerebral blood flow and metabolism : official journal of the International Society of Cerebral Blood Flow and Metabolism*. 1996; 16:834–40.
- Logan J, Fowler JS, Volkow ND, Wolf AP, Dewey SL, Schlyer DJ, MacGregor RR, Hitzemann R, Bendriem B, Gatley SJ, et al. Graphical analysis of reversible radioligand binding from time-activity measurements applied to [¹¹C-methyl]-(-)-cocaine PET studies in human subjects. *Journal of cerebral blood flow and metabolism : official journal of the International Society of Cerebral Blood Flow and Metabolism*. 1990; 10:740–7.

- Longo DL. Tumor heterogeneity and personalized medicine. *The New England journal of medicine*. 2012; 366:956–7. [PubMed: 22397658]
- Luo S, Zhang E, Su Y, Cheng T, Shi C. A review of NIR dyes in cancer targeting and imaging. *Biomaterials*. 2011; 32:7127–38. [PubMed: 21724249]
- Mach JP, Carrel S, Merenda C, Sordat B, Cerottini JC. In vivo localisation of radiolabelled antibodies to carcinoembryonic antigen in human colon carcinoma grafted into nude mice. *Nature*. 1974; 248:704–6. [PubMed: 4833275]
- Maeda H. The enhanced permeability and retention (EPR) effect in tumor vasculature: the key role of tumor-selective macromolecular drug targeting. *Advances in enzyme regulation*. 2001; 41:189–207. [PubMed: 11384745]
- Maeda H, Wu J, Sawa T, Matsumura Y, Hori K. Tumor vascular permeability and the EPR effect in macromolecular therapeutics: a review. *J Control Release*. 2000; 65:271–84. [PubMed: 10699287]
- Massoud TF, Gambhir SS. Molecular imaging in living subjects: seeing fundamental biological processes in a new light. *Genes & development*. 2003; 17:545–80. [PubMed: 12629038]
- Mattes MJ, Griffiths GL, Diril H, Goldenberg DM, Ong GL, Shih LB. Processing of antibody-radioisotope conjugates after binding to the surface of tumor cells. *Cancer*. 1994; 73:787–93. [PubMed: 8306261]
- Matzku S, Bruggen J, Brocker EB, Sorg C. Criteria for selecting monoclonal antibodies with respect to accumulation in melanoma tissue. *Cancer immunology, immunotherapy : CII*. 1987; 24:151–7. [PubMed: 3829049]
- McConahey PJ, Cerottini JC, Dixon FJ. An approach to the quantitation of immunogenic antigen. *The Journal of experimental medicine*. 1968; 127:1003–11. [PubMed: 5655099]
- McLarty K, Cornelissen B, Scollard DA, Done SJ, Chun K, Reilly RM. Associations between the uptake of (111)In-DTPA-trastuzumab, HER2 density and response to trastuzumab (Herceptin) in athymic mice bearing subcutaneous human tumour xenografts. *European journal of nuclear medicine and molecular imaging*. 2009; 36:81–93. [PubMed: 18712381]
- McPhaul JJ Jr, Dixon FJ. Characterization of human anti-glomerular basement membrane antibodies eluted from glomerulonephritic kidneys. *The Journal of clinical investigation*. 1970; 49:308–17. [PubMed: 4983662]
- Mikolajczyk K, Szabatin M, Rudnicki P, Grodzki M, Burger C. A JAVA environment for medical image data analysis: initial application for brain PET quantitation. *Med Inform*. 1998; 23:207–14.
- Mintun MA, Raichle ME, Kilbourn MR, Wooten GF, Welch MJ. A quantitative model for the in vivo assessment of drug binding sites with positron emission tomography. *Annals of neurology*. 1984; 15:217–27. [PubMed: 6609679]
- Mintun MA, Welch MJ, Siegel BA, Mathias CJ, Brodack JW, McGuire AH, Katzenellenbogen JA. Breast cancer: PET imaging of estrogen receptors. *Radiology*. 1988; 169:45–8. [PubMed: 3262228]
- Mortimer JE, Bading JR, Colcher DM, Conti PS, Frankel PH, Carroll MI, Tong S, Poku E, Miles JK, Shively JE, Raubitschek AA. Functional imaging of human epidermal growth factor receptor 2-positive metastatic breast cancer using (64)Cu-DOTA-trastuzumab PET. *Journal of nuclear medicine : official publication, Society of Nuclear Medicine*. 2014; 55:23–9.
- Muzic RF, Cornelius S. COMKAT: Compartment model kinetic analysis tool. *Journal of Nuclear Medicine*. 2001; 42:636–45. [PubMed: 11337554]
- Nagengast WB, de Vries EG, Hospers GA, Mulder NH, de Jong JR, Hollema H, Brouwers AH, van Dongen GA, Perk LR, Lub-de Hooge MN. In vivo VEGF imaging with radiolabeled bevacizumab in a human ovarian tumor xenograft. *Journal of nuclear medicine : official publication, Society of Nuclear Medicine*. 2007; 48:1313–9.
- Nakayama H, Kawase T, Okuda K, Wolff LF, Yoshie H. In-vivo near-infrared optical imaging of growing osteosarcoma cell lesions xenografted in mice: dual-channel quantitative evaluation of volume and mineralization. *Acta radiologica*. 2011; 52:978–88. [PubMed: 21969703]
- Ntziachristos V, Bremer C, Weissleder R. Fluorescence imaging with near-infrared light: new technological advances that enable in vivo molecular imaging. *European radiology*. 2003; 13:195–208. [PubMed: 12541130]

- Ntziachristos V, Ripoll J, Wang LV, Weissleder R. Looking and listening to light: the evolution of whole-body photonic imaging. *Nature biotechnology*. 2005; 23:313–20.
- Ohtake T, Kosaka N, Watanabe T, Yokoyama I, Moritan T, Masuo M, Iizuka M, Kozeni K, Momose T, Oku S, et al. Noninvasive method to obtain input function for measuring tissue glucose utilization of thoracic and abdominal organs. *Journal of nuclear medicine : official publication, Society of Nuclear Medicine*. 1991; 32:1432–8.
- Otsuji E, Yamaguchi T, Yamaoka N, Yamaguchi N, Imanishi J, Takahashi T. Biodistribution of monoclonal antibody A7 and its F(ab')₂ fragment in athymic nude mice bearing human pancreatic carcinoma. *Journal of surgical oncology*. 1992; 50:173–8. [PubMed: 1619940]
- Patlak CS, Blasberg RG. Graphical evaluation of blood-to-brain transfer constants from multiple-time uptake data. Generalizations. *Journal of cerebral blood flow and metabolism : official journal of the International Society of Cerebral Blood Flow and Metabolism*. 1985; 5:584–90.
- Patlak CS, Blasberg RG, Fenstermacher JD. Graphical evaluation of blood-to-brain transfer constants from multiple-time uptake data. *Journal of cerebral blood flow and metabolism : official journal of the International Society of Cerebral Blood Flow and Metabolism*. 1983; 3:1–7.
- Pogue BW, Samkoe KS, Hextrum S, O'Hara JA, Jermyn M, Srinivasan S, Hasan T. Imaging targeted-agent binding in vivo with two probes. *Journal of biomedical optics*. 2010; 15:030513. [PubMed: 20614996]
- Prabhakar U, Maeda H, Jain RK, Sevick-Muraca EM, Zamboni W, Farokhzad OC, Barry ST, Gabizon A, Grodzinski P, Blakey DC. Challenges and key considerations of the enhanced permeability and retention effect for nanomedicine drug delivery in oncology. *Cancer Res*. 2013; 73:2412–7. [PubMed: 23423979]
- Pressman D, Day ED, Blau M. The use of paired labeling in the determination of tumor-localizing antibodies. *Cancer Res*. 1957; 17:845–50. [PubMed: 13472674]
- Pruszyński M, Koumariou E, Vaidyanathan G, Revets H, Devoogdt N, Lahoutte T, Lysterly HK, Zalutsky MR. Improved tumor targeting of anti-HER2 nanobody through N-succinimidyl 4-guanidinomethyl-3-iodobenzoate radiolabeling. *Journal of nuclear medicine : official publication, Society of Nuclear Medicine*. 2014; 55:650–6.
- Raichle ME, Martin WR, Herscovitch P, Mintun MA, Markham J. Brain blood flow measured with intravenous H₂(15)O. II. Implementation and validation. *Journal of nuclear medicine : official publication, Society of Nuclear Medicine*. 1983; 24:790–8.
- Reist CJ, Archer GE, Kurpad SN, Wikstrand CJ, Vaidyanathan G, Willingham MC, Moscatello DK, Wong AJ, Bigner DD, Zalutsky MR. Tumor-specific anti-epidermal growth factor receptor variant III monoclonal antibodies: use of the tyramine-cellobiose radioiodination method enhances cellular retention and uptake in tumor xenografts. *Cancer Res*. 1995; 55:4375–82. [PubMed: 7671250]
- Reist CJ, Archer GE, Wikstrand CJ, Bigner DD, Zalutsky MR. Improved targeting of an anti-epidermal growth factor receptor variant III monoclonal antibody in tumor xenografts after labeling using N-succinimidyl 5-iodo-3-pyridinecarboxylate. *Cancer Res*. 1997; 57:1510–5. [PubMed: 9108453]
- Repetto-Llamazares A, Abbas N, Bruland OS, Dahle J, Larsen RH. Advantage of lutetium-177 versus radioiodine immunoconjugate in targeted radionuclide therapy of b-cell tumors. *Anticancer research*. 2014; 34:3263–9. [PubMed: 24982330]
- Rettig WJ, Old LJ. Immunogenetics of human cell surface differentiation. *Annual review of immunology*. 1989; 7:481–511.
- Robertson MW, Leslie CA, Bennett JP Jr. Apparent synaptic dopamine deficiency induced by withdrawal from chronic cocaine treatment. *Brain research*. 1991; 538:337–9. [PubMed: 2012975]
- Roholt O, Shaw A, Pressman D. Chemical differences between antibody fragments as shown by paired label studies. *Nature*. 1962; 196:773–4. [PubMed: 13982467]
- Rouzier R, Perou CM, Symmans WF, Ibrahim N, Cristofanilli M, Anderson K, Hess KR, Stec J, Ayers M, Wagner P, Morandi P, Fan C, Rabiul I, Ross JS, Hortobagyi GN, Puzstai L. Breast cancer molecular subtypes respond differently to preoperative chemotherapy. *Clinical cancer research :*

- an official journal of the American Association for Cancer Research. 2005; 11:5678–85. [PubMed: 16115903]
- Samkoe KS, Sexton K, Tichauer KM, Hextrum SK, Pardesi O, Davis SC, O'Hara JA, Hoopes PJ, Hasan T, Pogue BW. High vascular delivery of EGF, but low receptor binding rate is observed in AsPC-1 tumors as compared to normal pancreas. *Molecular imaging and biology : MIB : the official publication of the Academy of Molecular Imaging*. 2012; 14:472–9. [PubMed: 21847690]
- Samkoe KS, Tichauer KM, Gunn JR, Wells WA, Hasan T, Pogue BW. Quantitative in vivo immunohistochemistry of epidermal growth factor receptor using a receptor concentration imaging approach. *Cancer research*. 2014; 74:7465–74. [PubMed: 25344226]
- Sawle GV, Playford ED, Brooks DJ, Quinn N, Frackowiak RS. Asymmetrical pre-synaptic and post-synaptic changes in the striatal dopamine projection in dopa naive parkinsonism. Diagnostic implications of the D2 receptor status. *Brain : a journal of neurology*. 1993; 116(Pt 4):853–67. [PubMed: 8353712]
- Schiepers C, Chen W, Cloughesy T, Dahlbom M, Huang SC. 18F-FDOPA kinetics in brain tumors. *Journal of nuclear medicine : official publication, Society of Nuclear Medicine*. 2007; 48:1651–61.
- Schottelius M, Wester HJ. Molecular imaging targeting peptide receptors. *Methods*. 2009; 48:161–77. [PubMed: 19324088]
- Scott AM, Wolchok JD, Old LJ. Antibody therapy of cancer. *Nat Rev Cancer*. 2012; 12:278–87. [PubMed: 22437872]
- Sears DW, Wilson PH. Biochemical evidence for structurally distinct H-2Dd antigens differing in serological properties. *Immunogenetics*. 1981; 13:275–84. [PubMed: 6168578]
- Sevick-Muraca EM. Translation of near-infrared fluorescence imaging technologies: emerging clinical applications. *Annual review of medicine*. 2012; 63:217–31.
- Sevick-Muraca EM, Akers WJ, Joshi BP, Luker GD, Cutler CS, Marnett LJ, Contag CH, Wang TD, Azhdarinia A. Advancing the translation of optical imaging agents for clinical imaging. *Biomedical optics express*. 2013; 4:160–70. [PubMed: 23304655]
- Seymour LW. Passive Tumor Targeting of Soluble Macromolecules and Drug Conjugates. *Crit Rev Ther Drug*. 1992; 9:135–87.
- Shockley TR, Lin K, Sung C, Nagy JA, Tompkins RG, Dedrick RL, Dvorak HF, Yarmush ML. A quantitative analysis of tumor specific monoclonal antibody uptake by human melanoma xenografts: effects of antibody immunological properties and tumor antigen expression levels. *Cancer Res*. 1992; 52:357–66. [PubMed: 1728407]
- Sinha L, Wang Y, Yang C, Khan A, Brankov JG, Liu JTC, Tichauer KM. Quantification of the binding potential of cell-surface receptors in fresh excised specimens via dual-probe modeling of SERS nanoparticles. *Scientific reports*. 2015 in press.
- Stein R, Govindan SV, Chen S, Reed L, Richel H, Griffiths GL, Hansen HJ, Goldenberg DM. Radioimmunotherapy of a human lung cancer xenograft with monoclonal antibody RS7: evaluation of (177)Lu and comparison of its efficacy with that of (90)Y and residualizing (131)I. *Journal of nuclear medicine : official publication, Society of Nuclear Medicine*. 2001; 42:967–74.
- Stein R, Govindan SV, Mattes MJ, Chen S, Reed L, Newsome G, McBride BJ, Griffiths GL, Hansen HJ, Goldenberg DM. Improved iodine radiolabels for monoclonal antibody therapy. *Cancer Res*. 2003; 63:111–8. [PubMed: 12517786]
- Strauss LG. Fluorine-18 deoxyglucose and false-positive results: a major problem in the diagnostics of oncological patients. *European journal of nuclear medicine*. 1996; 23:1409–15. [PubMed: 8781149]
- Strauss LG, Koczan D, Seiz M, Tuettgenberg J, Schmieder K, Pan LY, Cheng CX, Dimitrakopoulou-Strauss A. Correlation of the Ga-68-Bombesin Analog Ga-68-BZH3 with Receptors Expression in Gliomas as Measured by Quantitative Dynamic Positron Emission Tomography (dPET) and Gene Arrays. *Molecular Imaging and Biology*. 2012; 14:376–83. [PubMed: 21744169]

- Sung C, Youle RJ, Dedrick RL. Pharmacokinetic analysis of immunotoxin uptake in solid tumors: role of plasma kinetics, capillary permeability, and binding. *Cancer Res.* 1990; 50:7382–92. [PubMed: 2224866]
- Tanigaki N, Yagi Y, Pressman D. Application of the paired label radioantibody technique to tissue sections and cell smears. *Journal of immunology.* 1967; 98:274–80.
- Terwisscha van Scheltinga AG, Lub-de Hooge MN, Abiraj K, Schroder CP, Pot L, Bossenmaier B, Thomas M, Holzlwimmer G, Friess T, Kosterink JG, de Vries EG. ImmunoPET and biodistribution with human epidermal growth factor receptor 3:targeting antibody (8)(9)Zr-RG7116. *mAbs.* 2014; 6:1051–8. [PubMed: 24870719]
- Thurber GM, Schmidt MM, Wittrup KD. Factors determining antibody distribution in tumors. *Trends in pharmacological sciences.* 2008; 29:57–61. [PubMed: 18179828]
- Thurber GM, Weissleder R. Quantitating antibody uptake in vivo: conditional dependence on antigen expression levels. *Molecular imaging and biology : MIB : the official publication of the Academy of Molecular Imaging.* 2011a; 13:623–32. [PubMed: 20809210]
- Thurber GM, Weissleder R. A systems approach for tumor pharmacokinetics. *PloS one.* 2011b; 6:e24696. [PubMed: 21935441]
- Tichauer KM, Deharvenjt SJ, Samkoe KS, Gunn JR, Bosenberg MW, Turk MJ, Hasan T, Stan RV, Pogue BW. Tumor endothelial marker imaging in melanomas using dual-tracer fluorescence molecular imaging. *Molecular imaging and biology : MIB : the official publication of the Academy of Molecular Imaging.* 2014a; 16:372–82. [PubMed: 24217944]
- Tichauer KM, Diop M, Elliott JT, Samkoe KS, Hasan T, Lawrence KS, Pogue BW. Accounting for pharmacokinetic differences in dual-tracer receptor density imaging. *Physics in medicine and biology.* 2014b; 59:2341–51. [PubMed: 24743262]
- Tichauer KM, Holt RW, El-Ghoussein F, Davis SC, Samkoe KS, Gunn JR, Leblond F, Pogue BW. Dual-tracer background subtraction approach for fluorescent molecular tomography. *Journal of biomedical optics.* 2013; 18:16003. [PubMed: 23292612]
- Tichauer KM, Samkoe KS, Gunn JR, Kanick SC, Hoopes PJ, Barth RJ, Kaufman PA, Hasan T, Pogue BW. Microscopic lymph node tumor burden quantified by macroscopic dual-tracer molecular imaging. *Nature medicine.* 2014c; 20:1348–53.
- Tichauer KM, Samkoe KS, Klubben WS, Hasan T, Pogue BW. Advantages of a dual-tracer model over reference tissue models for binding potential measurement in tumors. *Physics in medicine and biology.* 2012a; 57:6647–59. [PubMed: 23022732]
- Tichauer KM, Samkoe KS, Sexton KJ, Gunn JR, Hasan T, Pogue BW. Improved tumor contrast achieved by single time point dual-reporter fluorescence imaging. *Journal of biomedical optics.* 2012b; 17:066001. [PubMed: 22734757]
- Tichauer KM, Samkoe KS, Sexton KJ, Hextrum SK, Yang HH, Klubben WS, Gunn JR, Hasan T, Pogue BW. In vivo quantification of tumor receptor binding potential with dual-reporter molecular imaging. *Molecular imaging and biology : MIB : the official publication of the Academy of Molecular Imaging.* 2012c; 14:584–92. [PubMed: 22203241]
- Tolmachev V, Stone-Elander S, Orlova A. Radiolabelled receptor-tyrosine-kinase targeting drugs for patient stratification and monitoring of therapy response: prospects and pitfalls. *The lancet oncology.* 2010a; 11:992–1000. [PubMed: 20667780]
- Tolmachev V, Velikyan I, Sandstrom M, Orlova A. A HER2-binding Affibody molecule labelled with ⁶⁸Ga for PET imaging: direct in vivo comparison with the ¹¹¹In-labelled analogue. *European journal of nuclear medicine and molecular imaging.* 2010b; 37:1356–67. [PubMed: 20130858]
- Tomasi G, Kenny L, Mauri F, Turkheimer F, Aboagye EO. Quantification of receptor-ligand binding with [(1)(8)F]fluciclatide in metastatic breast cancer patients. *European journal of nuclear medicine and molecular imaging.* 2011; 38:2186–97. [PubMed: 21892622]
- Tomasi G, Turkheimer F, Aboagye E. Importance of quantification for the analysis of PET data in oncology: review of current methods and trends for the future. *Molecular imaging and biology : MIB : the official publication of the Academy of Molecular Imaging.* 2012; 14:131–46. [PubMed: 21842339]

- Vahrmeijer AL, Hutteman M, van der Vorst JR, van de Velde CJH, Frangioni JV. Image-guided cancer surgery using near-infrared fluorescence. *Nat Rev Clin Oncol*. 2013; 10:507–18. [PubMed: 23881033]
- Valdes PA, Leblond F, Jacobs VL, Wilson BC, Paulsen KD, Roberts DW. Quantitative, spectrally-resolved intraoperative fluorescence imaging. *Scientific reports*. 2012; 2:798. [PubMed: 23152935]
- van Dam GM, Themelis G, Crane LM, Harlaar NJ, Pleijhuis RG, Kelder W, Sarantopoulos A, de Jong JS, Arts HJ, van der Zee AG, Bart J, Low PS, Ntziachristos V. Intraoperative tumor-specific fluorescence imaging in ovarian cancer by folate receptor-alpha targeting: first in-human results. *Nature medicine*. 2011; 17:1315–9.
- Van Den Bossche B, Van de Wiele C. Receptor imaging in oncology by means of nuclear medicine: current status. *Journal of clinical oncology : official journal of the American Society of Clinical Oncology*. 2004; 22:3593–607. [PubMed: 15337810]
- van den Eynde, BJ.; Scott, AM. *Encyclopedia of Immunology*. Roitt, DPJ.; Roitt, IM., editors. London: Academic Press; 1998. p. 2424-31.
- Volkow ND, Fowler JS, Wang GJ, Dewey SL, Schlyer D, MacGregor R, Logan J, Alexoff D, Shea C, Hitzemann R, et al. Reproducibility of repeated measures of carbon-11-raclopride binding in the human brain. *Journal of nuclear medicine : official publication, Society of Nuclear Medicine*. 1993; 34:609–13.
- Wang D, Chen Y, Leigh SY, Haeberle H, Contag CH, Liu JT. Microscopic Delineation of Medulloblastoma Margins in a Transgenic Mouse Model Using a Topically Applied VEGFR-1 Probe. *Translational oncology*. 2012; 5:408–14. [PubMed: 23323155]
- Wang Y, Altaz K, Leigh SY, Wang D, Chen Y, Meza D, Liu JTC. Comprehensive spectral endoscopy of topically applied SERS nanoparticles in the rat esophagus. *Biomedical optics express*. 2014a; 5:2883. [PubMed: 25401005]
- Wang YW, Khan A, Som M, Wang D, Chen Y, Leigh SY, Meza D, McVeigh PZ, Wilson BC, Liu JT. Rapid ratiometric biomarker detection with topically applied SERS nanoparticles. *Technology*. 2014b; 2:118–32. [PubMed: 25045721]
- Weissleder R. Scaling down imaging: molecular mapping of cancer in mice. *Nat Rev Cancer*. 2002; 2:11–8. [PubMed: 11902581]
- Weissleder R. Molecular imaging in cancer. *Science*. 2006; 312:1168–71. [PubMed: 16728630]
- Weissleder R, Mahmood U. Molecular imaging. *Radiology*. 2001; 219:316–33. [PubMed: 11323453]
- Weissleder R, Pittet MJ. Imaging in the era of molecular oncology. *Nature*. 2008; 452:580–9. [PubMed: 18385732]
- Wikstrand CJ, McLendon RE, Bullard DE, Fredman P, Svennerholm L, Bigner DD. Production and characterization of two human glioma xenograft-localizing monoclonal antibodies. *Cancer Res*. 1986; 46:5933–40. [PubMed: 3756930]
- Wikstrand CJ, McLendon RE, Friedman AH, Bigner DD. Cell surface localization and density of the tumor-associated variant of the epidermal growth factor receptor, EGFRvIII. *Cancer Res*. 1997; 57:4130–40. [PubMed: 9307304]
- Wilks MQ, Knowles SM, Wu AM, Huang SC. Improved Modeling of In Vivo Kinetics of Slowly Diffusing Radiotracers for Tumor Imaging. *Journal of nuclear medicine : official publication, Society of Nuclear Medicine*. 2014
- Wilson CB, Dixon FJ. Quantitation of acute and chronic serum sickness in the rabbit. *The Journal of experimental medicine*. 1971; 134:7–18. [PubMed: 19867383]
- Wilson CB, Dixon FJ, Fortner JG, Cerilli GJ. Glomerular basement membrane--reactive antibody in anti-lymphocyte globulin. *The Journal of clinical investigation*. 1971; 50:1525–35. [PubMed: 4996886]
- Wittrup KD, Thurber GM, Schmidt MM, Rhoden JJ. Practical theoretic guidance for the design of tumor-targeting agents. *Methods in enzymology*. 2012; 503:255–68. [PubMed: 22230572]
- Wu AM, Senter PD. Arming antibodies: prospects and challenges for immunoconjugates. *Nature biotechnology*. 2005; 23:1137–46.

- Wu AM, Yazaki PJ. Designer genes: recombinant antibody fragments for biological imaging. *The quarterly journal of nuclear medicine : official publication of the Italian Association of Nuclear Medicine*. 2000; 44:268–83.
- Yang DJ, Kim EE, Inoue T. Targeted molecular imaging in oncology. *Annals of nuclear medicine*. 2006; 20:1–11. [PubMed: 16485568]
- Yokota S, Okazaki M, Yoshida M, Seon BK. Biodistribution and in vivo antitumor efficacy of the systemically administered anti-human T-leukemiaimmunotoxins and potentiation of their efficacy by alpha-interferon. *Leukemia research*. 1993; 17:69–79. [PubMed: 8429682]
- Zalutsky MR, Narula AS. A method for the radiohalogenation of proteins resulting in decreased thyroid uptake of radioiodine. *International journal of radiation applications and instrumentation. Part A, Applied radiation and isotopes*. 1987; 38:1051–5.
- Zavaleta C, de la Zerda A, Liu Z, Keren S, Cheng Z, Schipper M, Chen X, Dai H, Gambhir SS. Noninvasive Raman spectroscopy in living mice for evaluation of tumor targeting with carbon nanotubes. *Nano Lett*. 2008; 8:2800–5. [PubMed: 18683988]
- Zavaleta CL, Garai E, Liu JT, Sensarn S, Mandella MJ, Van de Sompel D, Friedland S, Van Dam J, Contag CH, Gambhir SS. A Raman-based endoscopic strategy for multiplexed molecular imaging. *Proceedings of the National Academy of Sciences of the United States of America*. 2013; 110:E2288–97. [PubMed: 23703909]
- Zavaleta CL, Smith BR, Walton I, Doering W, Davis G, Shojaei B, Natan MJ, Gambhir SS. Multiplexed imaging of surface enhanced Raman scattering nanotags in living mice using noninvasive Raman spectroscopy. *Proceedings of the National Academy of Sciences of the United States of America*. 2009; 106:13511–6. [PubMed: 19666578]
- Zhang X, Xiong Z, Wu Y, Cai W, Tseng JR, Gambhir SS, Chen X. Quantitative PET imaging of tumor integrin alphavbeta3 expression with 18F-FRGD2. *Journal of nuclear medicine : official publication, Society of Nuclear Medicine*. 2006; 47:113–21.
- Zhu L, Guo N, Li Q, Ma Y, Jacobson O, Lee S, Choi HS, Mansfield JR, Niu G, Chen X. Dynamic PET and Optical Imaging and Compartment Modeling using a Dual-labeled Cyclic RGD Peptide Probe. *Theranostics*. 2012; 2:746–56. [PubMed: 22916074]
- Zielinski R, Hassan M, Lyakhov I, Needle D, Chernomordik V, Garcia-Glaessner A, Ardeshirpour Y, Capala J, Gandjbakhche A. Affibody-DyLight conjugates for in vivo assessment of HER2 expression by near-infrared optical imaging. *PLoS one*. 2012; 7:e41016. [PubMed: 22911732]

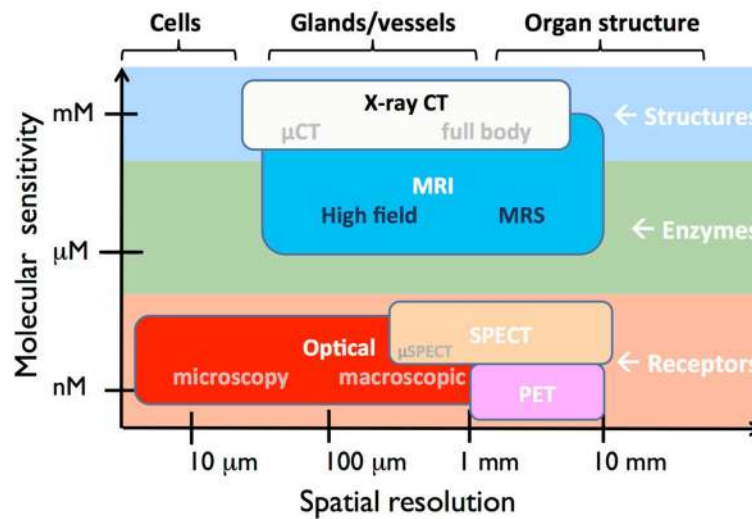


Figure 1.

Comparison of dominant medical imaging modalities with respect to molecular sensitivity (lowest concentration of an imaging reporter that can be accurately detected in a medium) and spatial resolution. Note that while optical imaging is capable of cellular and sub-cellular-level spatial resolution, this comes at the price of a reduced imaging depth in tissues (Leigh *et al.*, 2014).

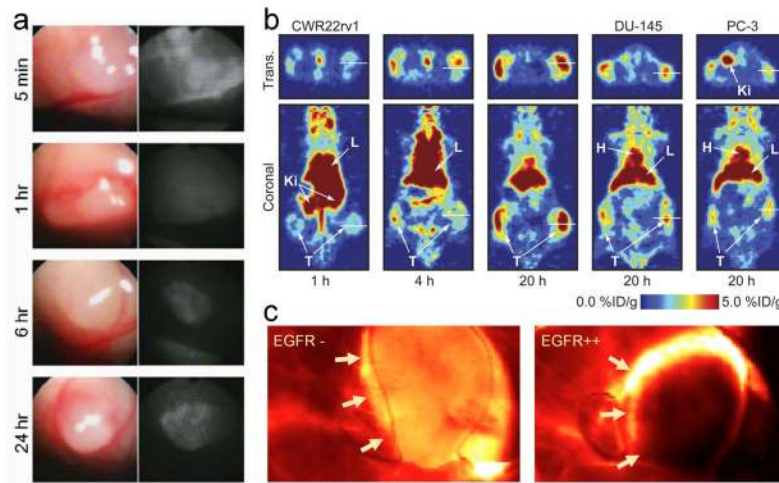
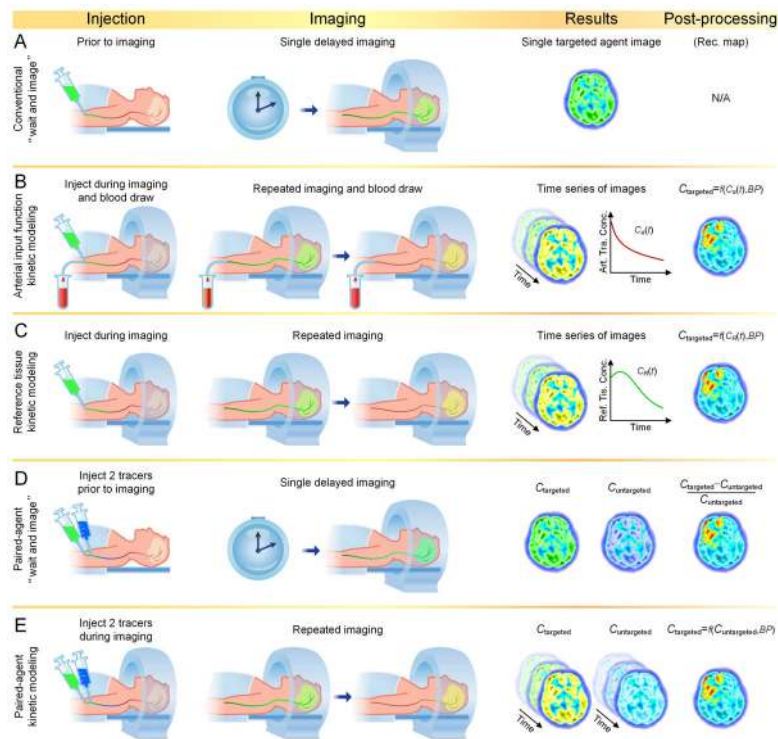


Figure 2. Variability of imaging-agent delivery and non-specific retention in tumors. (a) Example of an untargeted fluorescent imaging agent, indocyanine green (ICG), exhibiting preferential uptake and retention in an orthotopic mouse model of ovarian cancer. Obvious contrast can be seen by 6 h post-intravenous injection of the ICG (Kosaka *et al.*, 2011). (b) Transverse (Trans.) and coronal PET images of ⁸⁹Zr-labeled albumin – in three different tumor xenografts (CWR22rv1, DU-145, and PC-3) on the right and left flanks of mice – demonstrate large variability in enhanced permeability and retention (EPR) between tumor phenotypes (Heneweer *et al.*, 2011). (c) Fluorescence image of an epidermal growth factor receptor (EGFR)-targeted imaging agent in a tumor xenograft with no EGFR expression (EGFR-; left) and a tumor with high EGFR expression (EGFR++; right) at 1 h post injection. Overall tumor uptake was considerably higher in the EGFR- tumor compared to the EGFR++ tumor, demonstrating that nonspecific uptake confounds the relationship between targeted tracer uptake and receptor concentration (Tichauer *et al.*, 2012c). The locations of the tumors are indicated by the white arrows.

**Figure 3.**

Summary of methods to quantify cell-surface receptor concentrations *in vivo* using molecular imaging. Row A presents the dominant method in cancer imaging, the “wait and image” approach where a targeted imaging agent is injected and imaging is carried out after unbound agent is allowed to wash out. The imaged distribution of the remaining agent is presumed to reflect the distribution of the targeted receptor. Row B represents arterial-input-function-driven kinetic modeling of the temporal dynamics of a targeted imaging agent (from repeated imaging over time). Mathematical models associating tissue time-concentration curves with the arterial input function [$C_A(t)$] are used to estimate and map the binding potential (BP), a parameter that is proportional to receptor concentration. Such approaches typically require invasive arterial blood sampling during imaging and have troubles decoupling hemodynamic effects from specific-binding effects on the dynamics of imaging agents. Row C represents reference-tissue-input-function-driven kinetic modeling approaches that estimate BP by employing the time-concentration curve of a targeted imaging agent in a tissue devoid of targeted receptor [$C_R(t)$] as a surrogate of the arterial input function. Such approaches benefit from not requiring blood sampling; however, the hemodynamics of the reference tissue must be representative of all other tissues of interest for the approach to be relevant (a poor assumption for tumor imaging). Row D represents a “paired-agent” approach for estimating BP . This methodology requires the simultaneous injection of targeted and untargeted imaging agents that have similar kinetic characteristics and nonspecific binding properties. The concentration maps of the targeted imaging agent can be normalized by the map of the untargeted imaging agent to account for nonspecific effects and to calculate BP . Row E represents a more sophisticated version of the paired-agent approach illustrated in row D, using kinetic imaging data and the mathematical models

derived for reference-tissue-input imaging to estimate BP . This final method can provide the most accurate and precise estimations of BP if an ideal untargeted imaging agent is utilized that allows all nonspecific effects to be accounted for.

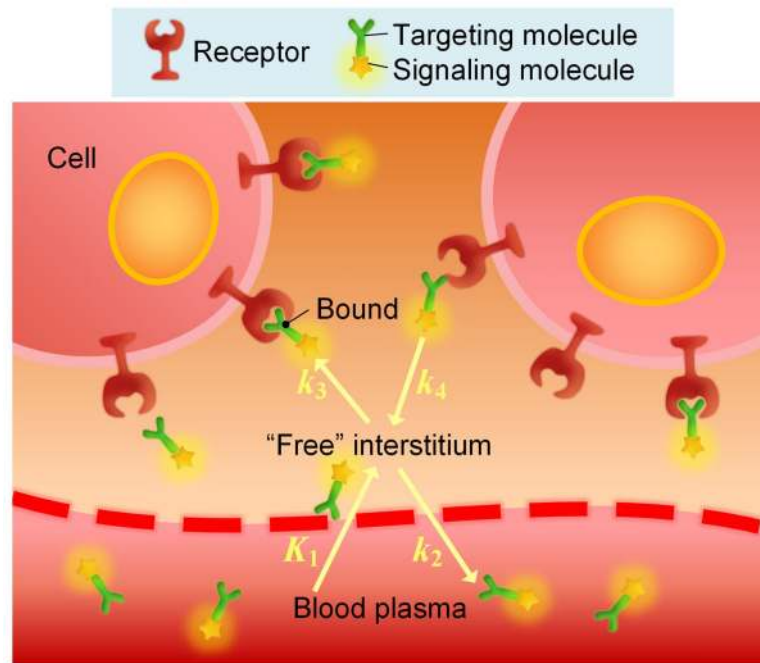
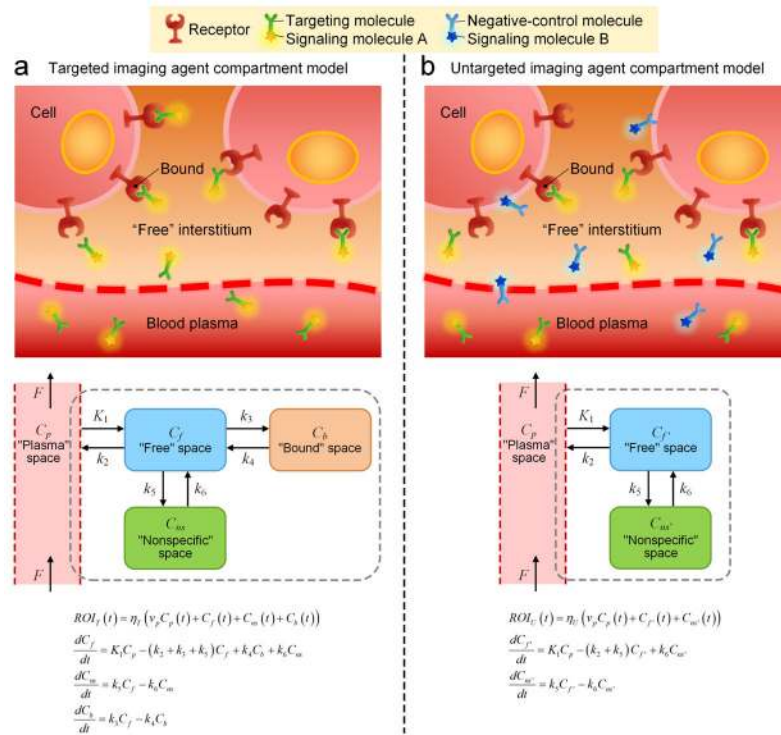


Figure 4. Distribution of a molecular targeted imaging agent in tissue. At any time, the concentration of an injected agent in tissue is in a dynamic balance between at least three “compartments:” the blood (specifically the blood plasma volume), the extravascular interstitial “free” space, and the “bound” space (bound to targeted cell-surface receptors). Rate constants K_1 and k_2 govern the rate of imaging agent delivery from the blood plasma to the tissue and washout of the agent from the tissue to the blood plasma, respectively. Rate constants k_3 and k_4 govern the rate of imaging agent receptor binding and receptor dissociation, respectively.

**Figure 5.**

Basic principles of kinetic compartment modeling of imaging agents that (a) reversibly target cell-surface receptors in tumors or (b) are used as untargeted controls. These form the basis for all kinetic modeling used to estimate or quantify cell-surface receptor concentrations. The drawings at the top illustrate where targeted and untargeted imaging agents are distributed in tissue (in this case, assuming no nonspecific binding). Compartment models are depicted in the box diagrams below the drawings. A three-compartment model is used for the targeted imaging agent while a two-compartment model (without specific binding) is utilized for the untargeted imaging agents. Both compartment models are driven by an input function that describes the concentration of the imaging agents in the blood plasma (C_p), which is assumed to be identical for the targeted and untargeted imaging agent. The rate constants K_1 and k_2 represent transport of the imaging agent from the blood plasma to the tissue and back, respectively. K_1 is intentionally capitalized to emphasize that it is unique from the other rate constants in that it can be dependent on the blood flow (F). The rate constants k_3/k_4 and k_5/k_6 govern association/dissociation of the agent with specific and nonspecific receptors, respectively (note: $k_4 = 0$ for irreversible binding). The dashed line encompassing the three tissue compartments, and a fraction of the blood plasma, reflects the fact that a pixel in a molecular image will include signal from all three compartments and part of the blood plasma (depending on the fractional volume of the pixel that is blood). The systems of equations can be solved in numerous ways to estimate or directly calculate the binding potential ($BP = k_3/k_4$), which is proportional to receptor concentration for agents that exhibit reversible binding, or to estimate k_3 , which is proportional to receptor concentration for agents that exhibit irreversible binding.

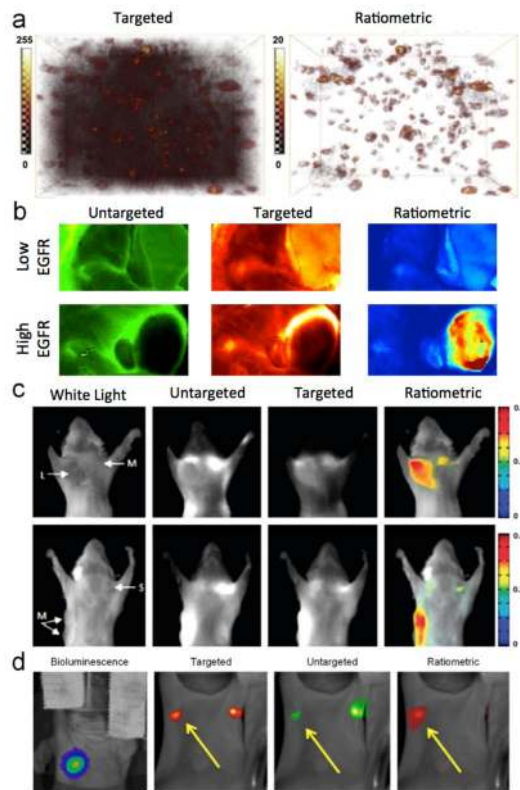


Figure 6. Paired-agent imaging applications. (a) Three-dimensional microscopy of a human epidermal growth factor receptor 2 (HER2)-targeted fluorescent contrast agent used to stain HER2-positive tumor cells suspended in a 3D matrix (Liu *et al.*, 2009). The left image shows the signal from the HER2-targeted imaging agent, displaying significant nonspecific uptake in the surrounding matrix. The figure on the right demonstrates that HER2-positive cells are more readily identified when normalizing the signal from the HER2-targeted imaging agent by the uptake of an untargeted imaging agent. (b) Temporal uptakes of an epidermal growth factor receptor (EGFR)-targeted imaging agent and an untargeted imaging agent in a low EGFR-expressing tumor line, 9L rat gliosarcoma (top row) and a high EGFR-expressing tumor line, A431 human epidermoid (bottom row). Higher retention of the targeted imaging agent is apparent in the low-EGFR tumor compared to the high-EGFR tumor. Quantitative analysis of the binding potential from the targeted (red-scale images) and untargeted imaging agents (green-scale images) can be used to map receptor concentration (Tichauer *et al.*, 2012c). (c) White-light images of large (L), medium (M), and small (S) tumors in a transgenic breast cancer mouse model (first column). Angiosense uptake, acting as an untargeted imaging agent, is presented in the second column. In the third column, either tumor-specific Prosense (top row) or MMPsense (bottom row) enzyme-activated fluorescence is visualized. Tumor location only becomes obvious by normalizing the enzyme-activated fluorescence images to the Angiosense images [fourth column of images] (Baeten *et al.*, 2009). (d) Application of paired-agent imaging for the detection of microscopic cancer burden in tumor-draining lymph nodes. A bioluminescence image on the left demonstrates the presence of metastatic bioluminescent human breast cancer tumor cells

in the right axillary lymph node of an athymic mouse. EGFR-targeted imaging agent uptake is similar in both the right and left axillary lymph nodes upon injection in the front footpad (second image); however, by normalizing the targeted agent uptake with untargeted agent uptake (third image), the affected lymph node is clearly delineated. As few as 200 cells were detectable using the paired-agent method in this model (Tichauer *et al.*, 2014c).

Table 1

List of publications from independent groups that have employed kinetic modeling to estimate cell-surface receptor concentrations *in vivo* in tumors (multiple instances are presented from the same group for unique kinetic models). Under the Approach column: the letters indicate the model in terms of the categorization established in Figure 3. B = arterial input function kinetic modeling, C = reference-tissue kinetic modeling, E = paired-agent kinetic modeling.

Publications	Modality/Application/Imaging	Agent/Receptor	Input function Approach
Daghighian <i>et al.</i> 1993 (Daghighian <i>et al.</i> , 1993)	PET/Human Glioma/ ¹²⁴ I-3F8 monoclonal antibody/Ganglioside GD2	Metabolite corrected blood sampling	B: Two-tissue compartment with assumed blood volume. 4 parameter fitting: K_1, k_2, k_3, k_4
Beattie <i>et al.</i> 2010 (Beattie <i>et al.</i> , 2010)	PET/Human Prostate Cancer/ ¹⁶ β- ¹⁸ F-Fluoro-5α-Dihydrotestosterone/ Androgen Receptor	Population derived metabolite corrected blood sampling with venous sample patient normalization	B: Comparison of 2, 4, and 6 parameter models: 1) V_p, k_{trap} ; 2) V_p, K_1, k_2, k_{trap} ; 3) $V_p, K_1, k_2, k_3, k_4, k_{trap}$
Cheal <i>et al.</i> 2014 (Cheal <i>et al.</i> , 2014)	PET/Mouse xenograft renal carcinoma/ ⁸⁹ Zr- and ¹²⁴ I-cG250/ carbonic anhydrase IX receptor	Image derived input function from heart ROI	B: Nonlinear two-tissue compartment model with 3 parameters: one-way extravasation/binding ($k_{2,1}$) dependent on saturation (nonlinear), internalization ($k_{3,2}$), and expulsion ($k_{0,3}$)
Gurfinkel <i>et al.</i> 2005 (Gurfinkel <i>et al.</i> , 2005)	Fluorescence Imaging/Mouse xenograft Kaposi's sarcoma/Cy5.5-c(KRGDF)/ $\alpha_v\beta_3$ integrin	Model based input function	B: Four parameter fit based on irreversible binding model.
Henze <i>et al.</i> 2005 (Henze <i>et al.</i> , 2005) and similar (Dimitrakopoulou-Strauss <i>et al.</i> , 2006; Dimitrakopoulou-Strauss <i>et al.</i> , 2011; Koukouraki <i>et al.</i> , 2006a; Koukouraki <i>et al.</i> , 2006b; Strauss <i>et al.</i> , 2012)	PET/Human Meningioma/ ⁶⁸ Ga-DOTA-D-Phe ¹ -Tyr ³ -Octreotide/Somatostatin receptor subtype 2	Image derived input function from arterial vessel(Ohtake <i>et al.</i> , 1991)	B: Two-tissue compartment with 5 parameter fitting using PMod software (PMod Technologies Ltd.) (Mikolajczyk <i>et al.</i> , 1998): V_p, K_1, k_2, k_3, k_4
Schiepers <i>et al.</i> 2007 (Schiepers <i>et al.</i> , 2007)	PET/Human Brain Tumors/ ¹⁸ F-FDOPA/Dopamine receptor	Blood sampling	B: Comparison of 6 different kinetic models/approaches
Ferl <i>et al.</i> 2009 (Ferl <i>et al.</i> , 2009)	PET/Various mouse xenografts/ ⁶⁴ Cu-DOTA-RGD/ $\alpha_v\beta_3$ integrin	Image-derived, from left ventricle of the heart	B: Two-tissue compartment model with 3–5 parameter fitting using SAAM II/PopKinetics software(Barrett <i>et al.</i> , 1998)
Wilks <i>et al.</i> 2014 (Wilks <i>et al.</i> , 2014)	PET/Mouse xenograft prostate cancer/ ¹²⁴ I-A11-minibody/Prostate stem cell antigen	Image derived input function from left ventricle of the heart	B: Two-tissue compartment model incorporating imaging agent diffusion for 6-parameter fit.
Tomasi <i>et al.</i> 2011 (Tomasi <i>et al.</i> , 2011)	PET/Human breast cancer/ ¹⁸ F]flucilatide/ $\alpha_v\beta_3$ integrin	Metabolite corrected blood sampling	B: Compared one-and two-tissue compartment models with 3–5 parameters as in Lammertsma <i>et al.</i> (Lammertsma <i>et al.</i> , 1996)
Bahce <i>et al.</i> 2013 (Bahce <i>et al.</i> , 2013)	PET/Human Non-small-cell lung cancer/ ¹¹ C]erlotinib/Epidermal growth factor receptor	Image-derived, from ascending aorta	B: Compared one-and two-tissue compartment models with 3–5 parameters as in Lammertsma <i>et al.</i> (Lammertsma <i>et al.</i> , 1996)
Buck <i>et al.</i> 2011 (Buck <i>et al.</i> , 2011)	PET/Rat glioma/ ¹⁸ F-N-fluoroacetyl-N-(2,5-dimethoxybenzyl)-2-phenoxaniline/Translocator protein (peripheral benzodiazepine receptor)	Metabolite corrected blood sampling	B: Logan graphical model(Logan <i>et al.</i> , 1990) to estimate Distribution Volume: $K_1/k_2(1+k_3/k_4)$
Beer <i>et al.</i> 2005 (Beer <i>et al.</i> , 2005) and 2007 (Beer <i>et al.</i> , 2007)	PET/Various human tumors/ ¹⁸ F]Galacto-RGD/ $\alpha_v\beta_3$ integrin	Image derived from largest artery in scan	B: Two-tissue compartment model for tumor using PMod software for fitting.

Publications	Modality/Application/Imaging	Agent/Receptor	Input function Approach
Zhang et al. 2006 (Zhang <i>et al.</i> , 2006) and similar (Guo <i>et al.</i> , 2012; Zhu <i>et al.</i> , 2012)	PET/Various mouse xenografts/[¹⁸ F]-FRGD2/ $\alpha_v\beta_3$ integrin	Muscle reference tissue input	C: Logan graphical reference tissue model(Logan <i>et al.</i> , 1996)
Chernomordik <i>et al.</i> 2010 (Chernomordik <i>et al.</i> , 2010) and similar (Ardeshirpour <i>et al.</i> , 2014; Hassan <i>et al.</i> , 2012; Zielinski <i>et al.</i> , 2012)	Fluorescence Imaging/Various xenografts/Alexa Fluor 750 –ABD-Z _{HER2:342}) ₂ -Cys Affibody/Human epidermal growth factor receptor-2 (HER2)	Modified Reference tissue from skin on contralateral side of subcutaneous tumor	C: Semi-graphical approach, extracting slope and asymptote from plot of normalized tumor-contralateral site temporal uptake data
Pogue et al. 2010 (Pogue <i>et al.</i> , 2010) <i>et al.</i> and similar (Samkoe <i>et al.</i> , 2012; Tichauer <i>et al.</i> , 2012b; Tichauer <i>et al.</i> , 2012c; Davis <i>et al.</i> , 2013; Hamzei <i>et al.</i> , 2014; Kanick <i>et al.</i> , 2014; Samkoe <i>et al.</i> , 2014; Tichauer <i>et al.</i> , 2014a; Tichauer <i>et al.</i> , 2014b; Tichauer <i>et al.</i> , 2013; Tichauer <i>et al.</i> , 2014c; Tichauer <i>et al.</i> , 2012a)	Fluorescence Imaging/Various xenografts/IRDye-800-EGF/Epidermal growth factor receptor (EGFR)	Untargeted imaging agent concentration-time curves (injected and imaged simultaneously with targeted imaging agent)	E: Various “reference tissue” mathematical models, replacing the reference tissue input with the untargeted imaging agent input functions.